Designing quinoline-isoniazid hybrids as potent anti-tubercular agents inhibiting mycolic acid biosynthesis

Matthéo Alcaraz, Bharvi Sharma, Françoise Roquet-Banères, Cyril Conde, Thierry Cochard, Franck Biet, Vipan Kumar, Laurent Kremer

Designing Quinoline-Isoniazid hybrids as potent anti-tubercular agents inhibiting mycolic acid biosynthesis

Matthéo Alcaraz[1]*, Bharvi Sharma[2]*, Françoise Roquet-Banères[1], Cyril Conde[3], Thierry Cochard[3], Franck Biet[3], Vipan Kumar[2,#], and Laurent Kremer[1,4,#]

[1]Centre National de la Recherche Scientifique UMR 9004, Institut de Recherche en Infectiologie de Montpellier (IRIM), Université de Montpellier, 1919 route de Mende, 34293, Montpellier, France.
[2]Department of Chemistry, Guru Nanak Dev University, Amritsar-143005, Punjab, India
[3]INRAE, Université de Tours, ISP, F-37380, Nouzilly, France
[4]INSERM, IRIM, 34293 Montpellier, France.

***These authors contributed equally to this work.**

[#]To whom correspondence should be addressed:

Tel: (+91) 183-258802 extn 3286; E-Mail: vipan_org@yahoo.com

Tel: (+33) 4 34 35 94 47; E-mail: laurent.kremer@irim.cnrs.fr

Running title: Anti-tubercular activity of quinoline-isoniazid hybrids

ABSTRACT

Isoniazid is a cornerstone of modern tuberculosis (TB) therapy and targets the enoyl ACP reductase InhA, a key enzyme in mycolic acid biosynthesis. InhA is still a promising target for the development of new anti-TB drugs. Herein, we report the design, synthesis, and anti-tubercular activity of new isoniazid hybrids. Among these, 1*H*-1,2,3 triazole-tethered quinoline-isoniazid conjugates **16a** to **16g** exhibited high activity against *Mycobacterium tuberculosis* with minimal inhibitory concentrations in the 0.25-0.50 µg/mL range and were bactericidal *in vitro*. Importantly, these compounds were well tolerated at high doses on mammalian cells, leading to high selectivity indices. The hybrids were dependent on functional KatG production to inhibit mycolic acid biosynthesis. Moreover, overexpression of InhA in *M. tuberculosis* resulted in high resistance levels to **16a**-**16g** and reduced mycolic acid biosynthesis inhibition, similar to isoniazid. Overall, these findings suggest that the synthesized quinoline-isoniazid hybrids are promising anti-tubercular molecules, which require further pre-clinical evaluation.

Keywords: *Mycobacterium tuberculosis*, drug resistance, quinoline-isoniazid hybrids, KatG, InhA, mycolic acids.

Abbreviations: ADMET, absorption, distribution, metabolism, excretion and toxicity; INH, isoniazid; MDR, multi-drug resistant; *Mtb*, *Mycobacterium tuberculosis*; RFB, rifabutin; SAR, structure-activity relationships; SI, selectivity index; TB, tuberculosis; TLC, thin-layer chromatography; XDR, extensive-drug resistant.

1. Introduction

Mycobacterium tuberculosis (*Mtb*), the pathogen responsible for the centuries-old infectious disease tuberculosis (TB), kills over 1.4 million people worldwide each year [1]. Since the beginning of 2020, the COVID-19 pandemic has had massive health, social, and economic consequences. As a result, the pandemic has threatened to reverse progress toward global TB targets. The WHO reported a 21% decrease in TB care and facilities since 2019, resulting in an estimated half-million additional TB-related deaths, slowing the decade-long progress toward the "End TB Strategy" [2]. The rise in animal-to-human transmission (zoonotic TB) and the increased risk of survival associated with co-infections such as HIV impedes the desired TB control [3,4]. Moreover, the emergence of multi-drug

resistant (MDR) and extensive-drug resistant (XDR)-TB strains, prolonged treatment regimens involving a combination of eight to ten drugs and the possibility of treatment failure highlight the severity of the situation and provide a strong impetus for the search for new anti-TB scaffolds [5,6]. Identifying new functional entities with improved permeability profiles is regarded as an ideal strategy for combating drug resistance [7–9]. Re-engineering of pre-existing anti-TB moieties/drugs, on the other hand, is seen as a more practical and efficient way to generate promising and safe anti-mycobacterial medications in a much shorter time [10].

Quinoline is an intriguing structural core found in a wide range of natural compounds, commercially available pharmaceuticals, and clinically approved anti-TB prospects like ciprofloxacin, levofloxacin, moxifloxacin, and gatifloxacin or bedaquiline (TMC207, Sirturo) **(Figure 1)** [11]. This latter has a diarylquinoline core and was approved by the US-FDA in 2012 to treat pulmonary MDR-TB after a 40-year wait. This ATP synthase inhibitor is very effective against both replicating and non-replicating strains [12]. However, side effects such as phospholipidosis induction at high concentrations, unexplained deaths, and deadly heart problems owing to QT interval prolongation limit its use [13]. The addition of functionalities such as oxadiazole (I) to the quinoline core has resulted in excellent anti-TB results [14]. Furthermore, the rapid use of hydroxychloroquinoline (HCQ) during the COVID-19 period has boosted the popularity of the quinoline core, which further strengthened the therapeutic potential of this moiety in the pharmaceutical sector.

Type II fatty acid synthase (FAS-II) enoyl-acyl carrier protein (ACP) reductase (InhA) is a validated target in anti-mycobacterial drug discovery. InhA is involved in synthesizing and elongating fatty acids to produce mycolic acids, the primary component of the mycobacterial cell wall [15–17]. The well-known anti-tubercular drug, Isoniazid (INH), is an InhA inhibitor [15]. The catalase-peroxidase (KatG) enzyme oxidizes INH to an isonicotinoyl radical that forms a covalent adduct (INH-NAD^+) with NADH [18–21]. This adduct inhibits InhA by binding to its catalytic domain, forming a ternary complex (InhA-isonicotinoyl-NADH) [22–24]. Consequently, the bacterial surface wrinkles and bulges, resulting in deformed and swollen rods that ultimately burst. It leads to disruption of mycolic acid biosynthesis and bacterial cell death [17,23]. However, the clinical use of INH in drug-resistant TB is limited due to mutations in either *katG* or *inhA* [25,26]. Further, the low permeability of INH (logP = -0.70) in *Mtb* granuloma has indicated its correlation with the longer duration of treatment [27,28]. In addition, the mycolic acid outer layer is too

hydrophobic to allow drugs to pass through efficiently, posing a risk of antibiotic deposition at the cell wall. As a result, chemically modulating INH with a lipophilic core (**II**) would enhance its diffusion through the cell envelope while preventing the generation of inactive metabolites produced after *N*-acetylation by the *N*-acetyl transferase (NAT) prior to KatG activation [29,30]. As a result, the chances of INH resistance are reduced.

We have previously described the 4-aminoquinoline-isoindoline-dione-INH triad's potent anti-mycobacterial activity (**III**, MIC = 6.0 μM) [31] **(Figure 1)**. The presence of quinoline and INH was critical for hybrids to inhibit bacterial growth. Furthermore, we reported the synthesis of isatin-bis-INH hybrids as promising bactericidal compounds with improved activity against intracellular *Mtb* compared to INH [32]. Herein, we decided to combine INH and its heterocyclic analogues (nicotinic acid hydrazide/pyrazine-2-carbohydrazide) with quinoline, keeping in mind the synergistic effect of lipophilicity for mycobacterial cell wall permeation (by introducing aryl core) and physicochemical parameters (by introducing triazole) required for effective drug-like properties. To develop a robust structure-activity relationship (SAR), we introduced a variety of linkers and varied the rigidity/flexibility on the synthesized hybrids. The success of the triazole core in anti-TB drug discovery is demonstrated by compound I-A09 (**IV**), which is currently in clinical studies [33] (**Figure 1**). In addition, nicotine- and pyrazine-based scaffolds were added in this investigation to evaluate their anti-mycobacterial potential to that of INH. Moreover, genetic and biochemical studies were also carried out to propose the mode of action of the most active hybrids by targeting InhA and inhibiting mycolic acid biosynthesis.

2. Results and discussion

2.1. Chemistry

The synthetic methodology involved the initial synthesis of 7-chloroquinoline based precursors **2, 5,** and **7**. For the synthesis of 4-azido-7-chloroquinoline **2**, 4,7-dichloroquinoline **1** was heated with NaN_3 in anhydrous DMF. The reaction of **1** with various alcohol amines (ethanolamine/propanolamine) produced **3**, which was then mesylated and azidated to form **4a-b** [34]. Propargylation of 4-piperazinyl-7-chloroquinoline **6** (obtained by reacting **1** with piperazine) in the presence of potassium carbonate and propargyl bromide afforded *N*-propargylated-piperazinyl-quinoline **7** [35] (**Scheme 1**).

The alkyne precursor **9**, was obtained by treating 4-hydroxybenzaldehyde/vanillin **8** with propargyl bromide in dry acetone. Cu-promoted azide-alkyne cycloaddition (CuAAC) between appropriate azides (**2** and **5**) and alkyne **9** yielded **12a-b** and **13a-d** with latent free aldehydic functionality. 2-azido-benzaldehyde **11** was synthesized by reacting 2-nitrobenzaldehyde with NaN_3 and HMPA (hexamethylphosphoramide). Click reaction of **11** with **7** in the presence of $CuSO_4.5H_2O$ and sodium ascorbate afforded **14** in excellent yield (**Scheme 2**).

The target hybrids *viz.* 7-chloroquinoline-isoniazid Schiff bases **16a-g** were synthesized by the condensation reaction of triazolylquinolines **12**-**14** with INH **15a** by heating in a microwave synthesizer (**Scheme 3**). The structures to the synthesized hybrids were assigned based on spectral data and analytical techniques. For instance, hybrid **16g** exhibited a molecular ion peak at *m/z* 552.1923 $[M+1]^+$ in its HRMS spectrum. In ^1H NMR, the presence of singlet at δ2.75 and 3.16 corresponding to methylene ($-CH_2$) protons of piperazine, singlet at δ3.79 corresponding to methylene ($-CH_2$) proton attached to triazole, singlets at δ8.19 and 8.51 corresponding to triazole and iminic protons, multiplet ranging between δ7.43-7.65 along with doublets at δ8.64 (J = 4.8 Hz) and 8.69 (J = 3.6 Hz), corresponding to INH (H^b and H^a) protons, together with other required numbers of protons favored the formation of **16g**. In addition, the appearance of characteristic absorption peaks at δ52.2, 52.7, 52.8, corresponding to methylene, and δ162.3 corresponding to amide carbons of INH in ^{13}C NMR confirmed the assigned structure.

Further, to compare the anti-mycobacterial activities of 7-chloroquinoline-isoniazids, the corresponding INH analogs, namely, nicotinic hydrazide **15b** and pyrazine-2-carbohydrazide **15c**, were incorporated to synthesize their complementary 7-chloroquinoline hybrids. The reaction resulted in the formation of 7-chloroquinoline-nicotinic hydrazones **17a-g** and 7-chloroquinoline-pyrazine hydrazones **18a-g**, as shown in **Scheme 4**.

2.2. Anti-mycobacterial activity and structure-activity relationship

We evaluated the synthesized library of compounds (precursors and the target hybrids) for their anti-mycobacterial activities against *Mtb* mc^26230, *M. marinum* (*Mma*) M strain, and *M. abscessus* (*Mab*) $CIP104536^T$ (S and R variants) using INH as a standard drug. The anti-mycobacterial activities, expressed as minimum inhibitory concentrations (MIC) are listed in **Table 1**. As apparent, even at the highest tested concentration of 200 μg/mL, most precursors, 1*H*-1,2,3-triazole tailored quinoline (**12**-**14**) with a free aldehydic group, were inactive on the tested strains. The inclusion of the INH core in

these precursors resulted in hybrids **16a-f** with MIC values ranging from 0.25-0.50 μg/mL. The MIC value of the hybrid **16a**, which has a triazole ring at the C-4 position of the quinoline core, was 0.25 μg/mL, which is in the same range as the MIC values reported for isatin-bis-INH conjugates [32]. The inclusion of a methoxy substituent at the *ortho*-position of the phenyl ring in **16b** resulted in decreased anti-mycobacterial activity with a MIC of 0.50 μg/mL. The presence of flexible linkers such as ethyl and propyl on the 4-aminoquinoline ring resulted in hybrids **16c-f** having anti-mycobacterial activities ranging from 0.25-0.50 μg/mL. Among these hybrids, **16f** having a propyl chain as a spacer and an *ortho*-anisyl ring proved to be the most potent with a MIC value of 0.25 μg/mL. Compound **16g** with a rigid piperazine ring at the C-4 position of quinoline again showed potent activity (MIC = 0.25 μg/mL). Additionally, two of the most promising compounds, **16d** and **16g,** exhibited MIC values of 50 μg/mL against *M. marinum*, two-fold lower potency than INH (25 μg/mL). The non-tuberculous *M. marinum* is closely affiliated to *M. tuberculosis* and is responsible for TB-like illness in fishes, frogs, and humans (upon exposure of injured skin to aqueous environment infected with the strain) [36]. *M. marinum*'s genetic similarity and pathology to human TB, as well as its improved safety profile for lab workers, make it an ideal surrogate model for studying *Mtb*. In addition, these hybrids failed to show any activity (MIC >200 μg/mL) against smooth or rough variants of *M. abscessus* (*Mab*) strains in the same manner as INH does (MIC >200 μg/mL). Pyrazine-2-carbohydrazide and nicotinic hydrazide were included in the present study to see if the anti-mycobacterial activity is attributable to hydrophilic INH. The lack of activity caused by pyrazine-2-carbohydrazide and nicotinic hydrazide confirmed INH's need to achieve good anti-mycobacterial outcomes. Generalized SAR in the graphical form is sketched in **Figure 2**.

To explore the safety, effectiveness, physicochemical characteristics, and drug-like properties of the most potent hybrids **16a-g,** we theoretically calculated ADMET studies (**Table S1**). Compound **16a** showed an intestinal absorption value of 100%, indicating its high oral bioavailability. Poor diffusion values (LogBB values ranging between -1.45 to -1.64) for permeating the blood-brain barrier subside the chances of side effects associated with the central nervous system. In addition, all the most potent compounds possess the potential to act as P-glycoprotein I and II inhibitors. The majority of the hybrids showed resistance to inhibition of most CYP450 isoforms, which increases the possibility of drug clearance and reduces the risk of drug-drug interactions and other negative side effects. These compounds had high lipophilicity values, with LogP > 3.95, good drug permeability, and solubilization. There was also an intriguing correlation between lipophilicity

(clogP) and anti-mycobacterial activity (MIC). In the case of **14**, for example, the addition of a lipophilic aryl moiety to quinoline-piperazinyl precursor **6** (clogP = 2.23, MIC = 92 μg/mL) resulted in decreased antimycobacterial activity (clogP = 3.60, MIC = 200 μg/mL). Except for quinoline-INH derivatives **16a-g**, converting free aldehyde to heterocyclic hydrazones had little effect on lipophilicity and anti-mycobacterial activity. Interestingly, conversion of precursor **6** (MIC = 92 μg/mL) to **16g** (MIC = 0.25 μg/mL) substantially increased the antimycobacterial activity by ~370 fold [37]. This could be attributed to the synergism between INH and the lipophilic aryl core, contributing to anti-mycobacterial potential and cell permeability.

It is also worth noting that the current framework **16f** (MIC = 0.25 μg/mL) with INH coupled *via* a hydrazone motif has 24 times the anti-TB activity than INH condensed to 4-aminoquinoline-isoindoline-dione motif III (**Figure 1**, MIC = 6.0 μM). As a result, the improved anti-mycobacterial effects in the current set of hybrids over the previously reported ones [32,37] highlight the importance of the existing structural framework in designing effective anti-mycobacterial agents.

2.3. Quinoline-INH conjugates (16a-g) are bactericidal against *M. tuberculosis*

We next investigated the bactericidal potency of the quinoline-INH hybrids (**16a-16g**) exhibiting low MIC values (0.25-0.50 μg/mL) towards *Mtb*. Bacterial cultures were individually treated with low concentrations of each **16a-16g** for 6 days, analogous to their respective MIC values that resulted in a deduction of kill curves by determining the colony-forming units (CFU). Exposure of the bacterial cultures to 1x MIC of the test compounds resulted in a progressive growth decline over time, likewise INH (**Figure 3A**). Increased concentration (5x MIC) of the test compounds caused a more rapid decrease in bacteria's growth during the first 3 days of treatment, whereas an appreciable 2-log reduction in CFU compared to the inoculum was achieved on day 6 (**Figure 3B**). An increase in dose to 20x MIC further improved the killing activity of the quinoline-INH hybrids (**16a-16g**) after 6 days of exposure to the compounds (~3-log reduction in CFU) but did not show a higher activity as compared to INH **(Figure 3C)**. Overall, these results suggest that hybrids **16a-g** exert a bactericidal activity comparable to INH against replicating *Mtb*.

2.4. *In vitro* cytotoxicity against macrophages

Many anti-TB drugs display toxicity toward eukaryotic cells. Herein, we evaluated the eventual cytotoxic activity of **16a-16g** in human THP-1 macrophages, incubated for 24 or 72 hrs with

increasing concentrations of each compound. INH and rifabutin (RFB) were used as internal control drugs. As shown in **Figure 4**, most compounds had a little effect on cell survival after 24 hrs of exposure, particularly at concentrations ≤ 10 µg/mL (CC_{50} > 100 µg/mL), except for **16g** (CC_{50} = 13 µg/mL). In general, **16a**, **16c**, **16d**, **16e**, **16f** showed reduced cytotoxicity compared to RFB (CC_{50} = 60 µg/mL) but higher cytotoxicity than INH, which did not alter cell survival at the highest concentration tested. Similar effects on cell survival were observed when testing cytotoxicity against Vero cells (**Figure S1**). Further exposure of THP-1 macrophage to the compounds for 72 hrs (**Figure 4**), **16g** appeared as the most cytotoxic compound (CC_{50} = 18 µg/mL), followed by **16c, 16d** and **16e** (CC_{50} = 34 µg/mL, 67 µg/mL and 73 µg/mL, respectively). With CC_{50} > 100 µg/mL, **16a**, **16b** and **16f** display selectivity indices (SI = CC_{50}/MIC) of > 200. Overall, these results indicate that most quinoline-INH hybrids are well tolerated at high doses on Vero kidney cells and macrophages, leading to high selectivity indices. The high SI is of particular interest for subsequent medicinal chemistry improvements to produce related compounds with augmented activity and biophysical properties, although some of the molecules already have shown good ADMET and physicochemical properties predictions.

2.5. Overexpression of InhA increases resistance to the quinoline-INH hybrids

Increased InhA expression or mutations that result in a decreased enzymatic affinity for binding to NADH are critical parameters in INH resistance. The covalent connection between INH and quinoline fragments in structural templates of hybrids **16a-g** causes substantial changes in the parent structure of INH either by imparting lipophilicity or by protecting the free NH_2 of INH. Consequently, it remains to be established whether the new hybrids share the exact mechanism of inhibition as INH by targeting InhA or follow a different pathway in the mechanism of action. The *inhA* gene of the FAS-II system was cloned under the control of the strong *hsp60* promoter into pMV261 [38], and the resulting plasmid was introduced into *Mtb* to explore whether **16a-g** inhibits the enoyl ACP reductase InhA of the FAS-II pathway [39]. The influence of InhA overexpression determined the MIC of **16a-g** on Middlebrook 7H9 broth and on Middlebrook 7H10 supplemented with OADC enrichment. Overexpression of *inhA* mediated high levels of resistance to each compound (25-fold enhanced MIC on pMV261-*inhA*) as compared to the control strain harboring the empty pMV261, similar to INH (20-fold enhanced MIC), and this was confirmed in both liquid

medium as well as on agar plates **(Table 2** and **Figure S2)**. Together, these results suggest that both INH and the INH hybrids share a similar mode of action, implicating the enoyl ACP reductase InhA.

2.6. 16g inhibits *de novo* synthesis of mycolic acids

We next assessed the mechanisms of action of the quinoline-INH hybrids by extracting the radioactive lipids from *Mtb* cultures treated for 15 hrs with increasing concentrations of INH (0.01, 0.05 and 0.25 µg/mL) or **16g** (0.05, 0.25 and 1.25 µg/mL) before labeling with 1 µCi/mL [^{14}C]acetate for an additional 7 hrs [40]. Mycolic acid methyl esters (MAMEs) were then separated and analyzed by thin-layer chromatography (TLC). Similar to INH, the production of the three mycolic acid classes (α*,* methoxy, keto) was altered in a dose-dependent manner **(Figure 5)**. Treatment with 1.25 µg/mL **16g** abolished mycolic biosynthesis, whereas the production of fatty acid methyl esters (FAMEs) remained unaffected. This indicates that, like INH, **16g** specifically inhibits FAS-II but not FAS-I, as expected for InhA inhibition. Notably, the mycolic acid profile of the recombinant strain carrying pMV261-*inhA* remained unaltered in the presence of 1.25 µg/mL **16g (Figure 5)**. This confirms that this strain is refractory to mycolic acid biosynthesis inhibition by **16g**, consistent with its high resistance level to **16g**. Overall, these observations are in line with specific inhibition of InhA, similarly to INH or isatin-bis-INH hybrids [32].

2.7. Strains resistant to 16d, 16f, and 16g are cross-resistant to INH and mutated in KatG

To assess the mechanisms of action of the hybrids and investigate their functional relatedness with INH, we selected spontaneously resistant strains of *Mtb* in the presence of 5x MIC or 20x MIC of either **16g** (designated strains Mtb-16g^{R}), **16f** (designated Mtb-16f^{R}) or **16d** (designated Mtb-16d^{R}). The resistance frequency to these inhibitors ranged from 1.16 x 10^{-6} to 7.1 x 10^{-7} **(Table 3)**. Each resistant mutant was highly cross-resistant to all other inhibitors as well as to INH, as defined by their very high resistance levels (MIC ≥ 200µg/mL) **(Table S2)**. That these strains remained susceptible to ethionamide (ETH), a drug that also targets InhA [15] **(Table S2)**, suggests that mutations do not occur in *inhA*, which was subsequently confirmed by sequencing the *inhA* gene and its promoter region and whole genome sequencing (data not shown).

Since resistance to INH is mainly driven by mutations in *katG* [41], this gene was sequenced in one clone selected for resistance on plates **(Table 3)**. Results indicate that single nucleotide polymorphisms (SNPs) occurred in *katG*. The resistor selected in the presence of 5 x MIC **16d**

harbored a single nucleotide insertion at position 665, resulting in a premature stop codon after residue 274. The mutant chosen in the presence of 20x MIC **16d** harbored a G495D aminoacid replacement while those selected with 5x MIC **16f** or **16g** harbored W161R and F594C single point mutations, respectively **(Table 3)**. Whole genome sequencing of mutant Mtb-16g$^{R}_{20X}$ revealed a 3.6 kb deletion ranging from position 2155554 to 2159232, comprising essentially *fadB5*, *lppC*, *Rv1910c*, *furA* and part of the *katG* gene **(Figure S3).** In addition, *Mtb* strains Mtb-11c^{R}, Mtb-11d^{R} and Mtb-INH^{R3} carrying the G421D, L430P, and W438Stop mutations in KatG, respectively [32], were growing in the presence of 1µg/mL **16a** to **16g**, while the parental strain failed to grow at these concentrations (**Figure S4**). Complementation of Mtb-11c^{R}, Mtb-11d^{R} and Mtb-INH^{R3} by introducing the pSMT3-*katG* [42] restored the susceptibility to INH as well as to **16a-g** (**Table S3**).

Overall, this confirms that mutations in KatG are prominent contributors of resistance to the quinoline-INH conjugates. The point mutations, insertions or large deletions reported here are different from those identified previously with isatin-bis-INH conjugates [32] and are not frequently detected in clinical strains resistant to INH [25,43]. Overall, these findings imply that the antimicrobial activity of quinoline-INH hybrids relies on KatG biotransformation, similarly to isatin-bis-INH hybrids [32].

We anticipate that further functional and structural studies should confirm the binding of **16a-g** to the KatG binding pocket and should help explain how these mutations affect the binding of quinoline-INH hybrids and the activity of KatG. However, since these compounds cannot overcome bioactivation by KatG, it can be inferred that they are probably less potent against INH-resistant clinical strains carrying mutations in *katG.* Although subsequent studies should investigate this point using a broad panel of clinical isolates resistant to INH, this may represent a limiting step compared to direct InhA inhibitors [44–48]. From a mechanistic point of view, these genetic studies indicate that the quinoline-INH hybrids, similarly to isatin-INH hybrids [32] or to INH, are pro-drugs that undergo biotransformation by KatG and, upon activation, are likely to react with NAD to generate the corresponding adducts, which in turn inhibit InhA activity, ultimately leading to mycolic acid cessation. That **16a** to **16g** appear completely inactive against *M. abscessus* **(Table 1)** is caused by the poor capacity of KatG$_{MAB}$ to activate the compounds, as previously shown for INH [49], further validating the KatG-dependent requirements of this family of compounds to be active. Collectively, these results provide strong evidence that quinoline-INH hybrids and isatin-INH hybrids share the same mode of bioactivation and action and that the mycolic acid pathway represents the primary

target of these compounds. In addition, despite sharing a quinoline core with fluoroquinolones or bedaquiline **(Figure 1)**, which are clinically used drugs targeting the DNA gyrase [50] or the ATP synthase [51], respectively, the most active quinoline-INH hybrids display another mode of action. Taken collectively, the comparison of the structures and mode of action of these families of molecules indicates that bioactivation and activity of INH-containing hybrids rely mainly on INH rather than on the other structural elements.

3. Conclusion

INH is one of the most effective first-intent anti-TB drugs and is still utilized as a scaffold for generating new compounds to fight TB. In this study, we have synthesized and explored the anti-mycobacterial efficacy of new quinoline-based heterocyclic hydrazones. Among these, quinoline-INH hybrids **16a-g** appeared to be the most promising ones with MIC values ranging from 0.25 to 0.50 μg/mL and 50 to >200 μg/mL against *Mtb* and *M. marinum,* respectively. In contrast, hybrids of quinoline with nicotinic acid hydrazide and pyrazine-2-carbohydrazide failed to elicit favorable results. The potent anti-tubercular INH-based chemical entities exert high *in vitro* killing activity against *Mtb* and displayed low toxicity against various mammalian cell types. The compounds are pro-drugs that require KatG activation to inhibit *de novo* synthesis of mycolic acids by targeting InhA. Substantially improved (370- and 24-fold) anti-mycobacterial activity of the current set of hybrids involving an appropriately arranged quinoline, triazole, and INH exemplifies the success of the present approach compared to previously reported quinoline-based hybrids [32,37]. Future studies are requested for the advancement of these compounds to the next level of *in vivo* studies.

4. Materials and Methods

4.1. Chemistry

4.1.1. General information

The reactions were performed by employing standard protocols and techniques. Schiff base condensation reactions were carried out on an Anton Paar Monowave-50 microwave reactor. Melting points were recorded using open capillaries and Stuart digital melting-point apparatus (SMP10) and uncorrected. JEOL (400 MHz) and Bruke rAvance II (500 MHz) spectrometers were used to record ^{1}H NMR spectra, and JEOL (100 MHz) and BrukerAvance II (125 MHz) spectrometers for ^{13}C NMR spectra with DMSO-d_6 as a solvent. The chemical shifts (δ) were expressed in parts per million (ppm)

and coupling constants (*J* values) were specified in hertz (Hz). Splitting patterns are designated as s: singlet, d: doublet, t: triplet, m: multiplet, dd: double of the doublet. Using ESI as the source, mass spectral data were assembled on Bruker high-resolution mass spectrometer (micrOTOF QII) equipment.

4.1.2. General procedure for the synthesis of conjugates 12-13

K_2CO_3 (1.2 mmol) was added to a well-stirred solution of 4-hydroxybenzaldehyde/ vanillin **8** (1mmol) in acetone, and the resulting mixture was stirred for 30 min at room temperature to generate anion. On addition of propargyl bromide (1 mmol), the reaction mixture was refluxed for 12 hrs. After completion of the reaction as monitored by TLC, $K_2CO_3$was filtered off, and acetone was evaporated under reduced pressure to yield *O*-propargylated benzaldehyde/*O*-propargylated vanillin **9** in excellent yields. The precursors **9** (1mmol) and 4-azido-7-chloroquinoline **2** (1mmol) were dissolved in EtOH: H_2O (8:2) mixture, and $CuSO_4.5H_2O$ (0.055 mmol) and sodium ascorbate (0.143 mmol) were added in a catalytic amount. The reaction mixture was stirred for 3 hrs at room temperature. After TLC monitoring of the reaction, the crude product was extracted with chloroform and water. The organic layer was dried with Na_2SO_4 and concentrated under reduced pressure to yield the desired hybrids **12a-b.** Compounds were purified by recrystallization using ethyl acetate: hexane (8:2) mixture. The same protocol was employed for the synthesis of target compounds **13a-d** with propargylated precursor **9** and azidoquinolines **5a-b**.

4.1.2.1. 4-((1-(7-chloroquinolin-4-yl)-1H-1,2,3-triazol-4-yl)methoxy)benzaldehyde (12a)

Yield 88%, pale white solid, MP = 194-196 ºC, ^{1}H NMR (500 MHz, DMSO-d_6) δ: 5.45 (s, 2H, -OCH_2), 7.31 (d, *J* = 8.4 Hz, 2H, Ar-H), 7.79 (d, *J* = 9.0 Hz, 1H, Ar-H), 7.85 (d, *J* = 4.5 Hz, 1H, Ar-H), 7.91 (d, *J* = 8.4 Hz, 2H, Ar-H), 7.99 (d, *J* = 9.1 Hz, 1H, Ar-H), 8.28 (s, 1H, triazole-H), 8.97 (s, 1H, Ar-H), 9.14 (d, *J* = 4.6 Hz, 1H, Ar-H), 9.88 (s, 1H, -CHO). ^{13}C NMR (100 MHz, DMSO-d_6) δ: 61.5, 115.7, 117.6, 120.7, 125.7, 127.5, 128.5, 129.5, 130.4, 132.3, 135.9, 140.7, 143.4, 149.7, 152.8, 163.3, 192.0. HRMS (ESI) calcd for $C_{19}H_{13}ClN_4O_2$ $[M+1]^+$ 365.0727, found 365.0745.

4.1.2.2 4-((1-(7-chloroquinolin-4-yl)-1H-1,2,3-triazol-4-yl)methoxy)-3-methoxybenzaldehyde (12b)

Yield 84%, pale white solid, MP = 193-195 ºC, ^{1}H NMR (400 MHz, DMSO-d_6)δ: 3.74 (s, 3H, -OCH_3), 5.40 (s, 2H, -OCH_2), 6.43 (d, *J* = 5.4 Hz, 1H, Ar-H), 7.31-7.37 (m, 2H, Ar-H), 7.42 (dd, *J* =

8.9, 2.0 Hz, 1H, Ar-H), 7.49 (dd, *J* = 8.5, 1.9 Hz, 1H, Ar-H), 7.78 (d, *J* = 1.9 Hz, 1H, Ar-H), 8.25 (d, *J* = 9.1 Hz, 1H, Ar-H), 8.29 (s, 1H, triazole-H), 8.37 (d, *J* = 5.2 Hz, 1H, Ar-H), 9.88 (s, 1H, -CHO). ^{13}C NMR (125 MHz, DMSO-d_6) δ: 55.9, 61.7, 109.3, 114.6, 115.6, 117.4, 120.7, 122.4, 125.4, 128.3, 129.5, 135.8, 140.6, 143.7, 144.5, 149.6, 152.9, 162.9, 192.1. HRMS (ESI) calcd for $C_{20}H_{15}ClN_4O_3$ $[M+1]^+$ 395.0833, found 395.0865.

4.1.2.3. 4-((1-(2-((7-chloroquinolin-4-yl)amino)ethyl)-1H-1,2,3-triazol-4-yl)methoxy)benzaldehyde (13a)

Yield 84%, pale white solid, MP = 103-107 °C, ^{1}H NMR (400 MHz, DMSO- d_6) δ: 3.84 (s, 3H, -CH_2+NH (exchangeable with D_2O)),4.69 (s, 2H, -CH_2), 5.17 (s, 2H, -OCH_2), 7.35 (d, *J* = 8.3 Hz, 2H, Ar-H), 7.81 (d, *J* = 9.1 Hz, 1H, Ar-H), 7.86 (d, *J* = 4.3 Hz, 1H, Ar-H), 7.93 (d, *J* = 8.3 Hz, 2H, Ar-H), 8.01 (d, *J* = 9.1 Hz, 1H, Ar-H), 8.29 (s, 1H, triazole-H), 8.98 (s, 1H, Ar-H), 9.15 (d, *J* = 4.4 Hz, 1H, Ar-H), 9.87 (s, 1H, -CHO).^{13}C NMR (100 MHz, DMSO-d_6)δ: 42.7, 48.1, 61.9, 115.7, 116.2, 124.3, 125.1, 125.3, 125.9, 130.1, 132.3, 132.7, 135.9, 142.2, 152.8, 163.3, 191.8. HRMS (ESI) calcd for $C_{21}H_{18}ClN_5O_2$ $[M+1]^+$ 408.1149, found 408.1112.

4.1.2.4. 4-((1-(3-((7-chloroquinolin-4-yl)amino)propyl)-1H-1,2,3-triazol-4-yl)methoxy)benzaldehyde (13b)

Yield 82%, brown semisolid, ^{1}H NMR (400 MHz, DMSO-d_6) δ: 2.18-2.25 (m, 2H, -CH_2), 3.33-3.38 (m, 3H, -CH_2 +-NH (exchangeable with D_2O)), 4.50 (t, *J* = 6.9 Hz, 2H, -CH_2), 5.20 (s, 2H, -OCH_2), 6.57 (s, 1H, Ar-H), 7.17 (d, *J* = 8.7 Hz, 2H, Ar-H), 7.51 (d, *J* = 9.0 Hz, 1H, Ar-H), 7.82 (d, *J* = 8.7 Hz, 3H, Ar-H), 8.22 (d, *J* = 6.6 Hz, 1H, Ar-H), 8.28 (s, 1H, triazole-H), 8.36 (d, *J* = 8.5 Hz, 1H, Ar-H), 9.82 (s, 1H, -CHO). ^{13}C NMR (100 MHz, DMSO-d_6) δ: 28.7, 40.5, 47.9, 61.9, 115.6, 116.3, 124.3, 125.3, 125.4, 125.8, 130.3, 132.3, 132.5, 135.9, 142.5, 152.7, 163.4, 191.8. HRMS (ESI) calcd for $C_{22}H_{20}ClN_5O_2$ $[M+1]^+$ 422.1306, found 422.1364.

4.1.2.5. 4-((1-(2-((7-chloroquinolin-4-yl)amino)ethyl)-1H-1,2,3-triazol-4-yl)methoxy)-3-methoxybenzaldehyde (13c)

Yield 84%, pale white solid, MP = 203-205 °C, ^{1}H NMR (400 MHz, DMSO-d_6) δ:3.32-3.36 (m, 3H, -CH_2 +-NH (exchangeable with D_2O)), 3.76 (s, 3H, -OCH_3), 4.54 (t, *J* = 7.1 Hz, 2H, -CH_2), 5.24 (s, 2H, -OCH_2), 6.45 (d, *J* = 5.4 Hz, 1H, Ar-H), 7.29-7.35 (m, 2H, Ar-H), 7.41 (dd, *J* = 8.7, 2.0 Hz, 1H,

Ar-H), 7.51 (dd, *J* = 8.5, 1.9 Hz, 1H, Ar-H), 7.79 (d, *J* = 1.9 Hz, 1H, Ar-H), 8.24 (d, *J* = 9.0 Hz, 1H, Ar-H), 8.30 (s, 1H, triazole-H), 8.36 (d, *J* = 5.2 Hz, 1H, Ar-H), 9.86 (s, 1H, -CHO).^{13}C NMR (100 MHz, DMSO-d_6) *δ*: 42.8, 48.3, 61.9, 100.1, 110.3, 113.4, 117.5, 124.5, 124.6, 125.7, 126.2, 127.1, 130.5, 134.2, 142.3, 148.6, 149.6, 150.2, 151.7, 153.2, 192.0. HRMS (ESI) calcd for $C_{22}H_{20}ClN_5O_3$ $[M+1]^+$ 438.1255, found 438.1205.

4.1.2.6. 4-((1-(3-((7-chloroquinolin-4-yl)amino)propyl)-1H-1,2,3-triazol-4-yl)methoxy)-3 methoxybenzaldehyde (13d)

Yield 86%, brown semisolid, ^{1}H NMR (400 MHz, DMSO-d_6) *δ*: 2.16-2.24 (m, 2H, -CH_2-), 3.25-3.30 (m, 3H, -CH_2- + -NH (exchangeable with D_2O)), 3.76 (s, 3H, -OCH_3), 4.50 (t, *J* = 6.9 Hz, 2H, -CH_2), 5.21 (s, 2H, -OCH_2), 6.41 (d, *J* = 5.5 Hz, 1H, Ar-H), 7.33-7.39 (m, 2H, Ar-H), 7.44 (dd, *J* = 9.0, 2.0 Hz, 1H, Ar-H), 7.51 (dd, *J* = 8.3, 1.7 Hz, 1H, Ar-H), 7.76 (d, *J* = 1.9 Hz, 1H, Ar-H), 8.23 (d, *J* = 9.0 Hz, 1H, Ar-H), 8.28 (s, 1H, triazole-H), 8.36 (d, *J* = 5.0 Hz, 1H, Ar-H), 9.80 (s, 1H, -CHO).^{13}C NMR (100 MHz, DMSO-d_6)*δ*: 28.9, 47.9, 55.9, 62.2, 99.2, 110.1, 113.0, 117.8, 124.7, 124.8, 125.6, 126.3, 127.3, 130.4, 134.3, 142.5, 148.7, 149.7, 150.8, 151.8, 153.3, 191.9. HRMS (ESI) calcd for $C_{23}H_{22}ClN_5O_3$ $[M+1]^+$ 452.1411, found 452.1473.

4.1.3. General procedure for the synthesis of conjugates 14

To a well-stirred solution of *O*-nitrobenzaldehyde**10** (1 mmol) in HMPA, NaN_3 (2 mmol) was added, and the resulting mixture was heated at 60 ^oC for 5-6 hrs. After completion of the reaction, the reaction mixture was extracted with ether and ice-cold water. The organic layer was dried over Na_2SO_4 and concentrated under reduced pressure to afford **11**. *O*-azido-benzaldehyde **11** and N-propargylated-piperazinylquinoline **7** were dissolved in ethanol:H_2O (8:2) along with subsequent addition of a catalytic amount of $CuSO_4.5H_2O$ (0.055 mmol) and sodium ascorbate (0.143 mmol). The reaction mixture was stirred for 3 hrs at room temperature. After the reaction as monitored by TLC, the crude product was extracted with chloroform and water. The organic layer was dried with Na_2SO_4 and then concentrated under reduced pressure to yield the desired conjugates **14.** Compounds were purified by column chromatography using silica gel (60–120 mesh) and ethyl acetate: hexane (8:3) mixture.

4.1.3.1. 2-(4-((4-(7-chloroquinolin-4-yl)piperazin-1-yl)methyl)-1H-1,2,3-triazol-1-yl)benzaldehyde (14)

Yield 87%, brown semisolid, ^{1}H NMR (400 MHz,$CDCl_3$) δ: 2.87 (s, 4H, -CH_2), 3.25 (s, 4H, -CH_2), 3.91 (s, 2H, -CH_2), 6.81 (d, *J* = 3.3 Hz, 1H, Ar-H), 7.39 (d, *J* = 8.9 Hz, 1H, Ar-H), 7.53 (d, *J* = 7.9 Hz, 1H, Ar-H), 7.65 (t, *J* = 7.5 Hz, 1H, Ar-H), 7.75 (td, *J* = 7.7, 1.5 Hz,1H, Ar-H), 7.90-8.00 (m, 4H, triazole-H + 3Ar-H), 8.08 (dd, *J* = 7.7, 1.3 Hz, 1H, Ar-H), 9.90 (s, 1H, -CHO). ^{13}C NMR (100 MHz, $CDCl_3$) δ: 52.0, 52.9, 53.1, 109.1, 125.0, 125.3, 125.5, 126.3, 128.8, 129.9, 130.2, 130.3, 134.8, 135.0, 145.0, 151.9, 156.9, 188.6. HRMS (ESI) calcd for $C_{23}H_{21}ClN_6O$ $[M+1]^+$ 433.1465, found 433.1412.

4.1.4. General procedure for the synthesis of conjugates 16-18

Conjugates **16a-g** were synthesized by subjecting **12-14** (1 mmol) and INH (1mmol) to microwave irradiation at 100 ^{o}C for 15-20 min in ethanol as a solvent. **16a-g** precipitated out from reaction mixture upon cooling the mixture, which upon filtration and washing with ether afforded pure **16a-g** in excellent yields. The same protocol was applied for the synthesis of hybrids **17, 18.**

4.1.4.1. (E)-N'-(4-((1-(7-chloroquinolin-4-yl)-1H-1,2,3-triazol-4 yl)methoxy)benzylidene) isonicotinohydrazide (16a)

Yield 74%, pale white solid, MP = 230-232^{o}C, ^{1}H NMR (500 MHz, DMSO-d_6)δ: 5.38 (s, 2H, -OCH_2), 7.20 (d, *J* = 8.4 Hz, 2H, Ar-H), 7.74-7.81 (m, 5H, 2H^b + 3Ar-H), 7.83 (d, *J* = 4.5 Hz, 1H, Ar-H), 7.98 (d, *J* = 9.1 Hz, 1H, Ar-H), 8.26 (s, 1H, triazole-H), 8.39 (s, 1H, -CH=N), 8.77 (s, 2H, H^a), 8.95 (s, 1H, Ar-H), 9.13 (d, *J* = 4.5 Hz, 1H, Ar-H), 12.02 (s, 1H, -NH (exchangeable with D_2O)). ^{13}C NMR (125 MHz, DMSO-d_6) δ: 61.3, 115.6, 117.5, 120.7, 122.0, 125.7, 127.4, 128.4, 129.5, 135.9, 140.7, 140.9, 143.8, 149.5, 149.7, 150.7, 152.8, 160.2, 162.1. HRMS (ESI) calcd for $C_{25}H_{18}ClN_7O_2$ $[M+1]^+$ 484.1211, found 484.1256.

4.1.4.2. (E)-N'-(4-((1-(7-chloroquinolin-4-yl)-1H-1,2,3-triazol-4-yl)methoxy)-3-methoxybenzylidene)isonicotinohydrazide (16b)

Yield 73%, light brown solid, MP = 188-190^{o}C, ^{1}H NMR (500 MHz, DMSO-d_6)δ: 3.81 (s,3H, OCH_3), 5.19 (s, 2H, -OCH_2), 6.72 (d, *J* = 5.3 Hz, 1H Ar-H), 7.20-7.23 (m, 2H, Ar-H), 7.41 (s, 1H, Ar-H), 7.67 (d, *J* = 8.3 Hz, 1H, Ar-H), 7.79-7.85 (m, 4H, 2H^b +3Ar-H), 8.29 (s, 1H, triazole-H),

8.39-8.41 (m, 2H, -CH=N+Ar-H), 8.78 (d, *J* = 5.1 Hz, 2H, H^a), 12.01 (s, 1H, -NH (exchangeable with D_2O)). ^{13}C NMR (125 MHz, DMSO-d_6) δ: 55.8, 61.9, 109.3, 113.9, 117.9, 120.4, 121.2, 122.7, 125.9, 127.5, 127.8, 128.5, 129.4, 135.8, 140.7, 143.2, 144.2, 148.1, 149.7, 150.8, 152.7, 160.1, 162.9. HRMS (ESI) calcd for $C_{26}H_{20}ClN_7O_3$ $[M+1]^+$ 514.1316, found 514.1372.

4.1.4.3.(E)-N'-(4-((1-(2-((7-chloroquinolin-4-yl)amino)ethyl)-1H-1,2,3-triazol-4-yl)methoxy)benzylidene)isonicotinohydrazide (16c)

Yield 72% , pale white solid, MP = 196-198°C, ^1H NMR (500 MHz, DMSO-d_6) δ: 3.84-3.86 (m, 2H, -CH_2), 4.72 (s, 2H, -CH_2), 5.29 (s, 2H, -OCH_2), 6.95 (s, 1H, -NH (exchangeable with D_2O)), 7.25 (d, *J* = 8.3 Hz, 2H, Ar-H), 7.71-7.79 (m, 5H, $2H^b$ + 3Ar-H), 7.89 (d, *J* = 4.4 Hz, 1H, Ar-H), 7.98 (d, *J* = 9.1 Hz, 1H, Ar-H), 8.29 (s, 1H, triazole-H), 8.37 (s, 1H, -CH=N), 8.79 (s, 2H, H^a), 8.96 (s, 1H, Ar-H), 9.12 (d, *J* = 4.5 Hz, 1H, Ar-H), 12.01 (s, 1H, -NH (exchangeable with D_2O)). ^{13}C NMR (125 MHz, DMSO-d_6) δ: 42.8, 48.1, 61.7, 115.7, 117.9, 120.8, 121.2, 125.6, 127.3, 128.1, 129.6, 134.9, 140.1, 140.9, 143.7, 149.6, 149.9, 150.3, 152.9, 160.1, 162.4. HRMS (ESI) calcd for $C_{27}H_{23}ClN_8O_2$ $[M+1]^+$ 527.1632, found 527.1681.

4.1.4.4.(E)-N'-(4-((1-(3-((7-chloroquinolin-4-yl)amino)propyl)-1H-1,2,3-triazol-4-yl)methoxy)benzylidene)isonicotinohydrazide (16d)

Yield 75%, pale white solid, MP = 148-150°C, ^1H NMR (400 MHz, DMSO-d_6) δ: 2.17-2.23 (m, 2H, -CH_2), 4.49 (t, *J* = 6.9 Hz, 2H, -CH_2), 5.16 (s, 2H, -OCH_2), 6.44 (d, *J* = 5.7 Hz, 1H, Ar-H), 7.09 (d, *J* = 8.7 Hz, 2H, Ar-H), 7.46 (dd, *J* = 9.0, 2.1 Hz, 1H, Ar-H), 7.65-7.68 (m, 3H, Ar-H), 7.76-7.78 (m, 4H, $2H^b$ +2Ar-H), 8.26 (s, 1H, triazole-H), 8.36-8.37 (m, 2H, -CH=N + -NH (exchangeable with D_2O)), 8.73 (d, *J* = 5.5 Hz, 2H, INH), 11.94 (s, 1H, -NH (exchangeable with D_2O)). ^{13}C NMR (125 MHz, DMSO-d_6) δ: 28.6, 47.7, 49.3, 61.8, 115.6, 116.4, 119.9, 121.4, 125.3, 126.9, 127.2, 128.9, 130.1, 135.1, 140.1, 140.3, 142.9, 148.9, 149.8, 150.2, 152.7, 158.2, 162.2. HRMS (ESI) calcd for $C_{28}H_{25}ClN_8O_2$ $[M+1]^+$ 541.1789, found 541.1724.

4.1.4.5. (E)-N'-(4-((1-(2-((7-chloroquinolin-4-yl)amino)ethyl)-1H-1,2,3-triazol-4-yl)methoxy)-3-methoxybenzylidene)isonicotinohydrazide (16e)

Yield 73%, light brown solid, MP = 183-185°C, ^1H NMR (400 MHz, DMSO-d_6) δ: 3.24-2.83 (m, 3H, -CH_2+NH (exchangeable with D_2O)), 3.81 (s, 3H, -OCH_3), 4.71 (s, 2H, -CH_2), 5.17 (s, 2H, -OCH_2),

6.78 (d, *J* = 5.1 Hz, 1H Ar-H), 7.21 (dd, *J* = 18.5 Hz, 6.2 Hz, 2H, Ar-H), 7.41 (s, 1H, Ar-H), 7.64 (d, *J* = 8.4 Hz, 1H, Ar-H), 7.78-7.83 (m, 5H, $2H^b$ +3Ar-H), 8.27 (s, 1H, triazole-H), 8.38 (s, 1H, -CH=N), 8.77 (d, *J* = 5.1 Hz, 2H, H^a), 12.01 (s, 1H, -NH (exchangeable with D_2O)). ^{13}C NMR (100 MHz, DMSO-d_6)δ: 42.6, 48.3, 55.8, 61.9, 109.3, 113.4, 117.9, 120.9, 121.3, 122.7, 125.9, 127.5, 127.9, 129.5, 135.6, 140.7, 143.1, 144.3, 148.2, 149.6, 150.9, 152.7, 160.2, 162.9. HRMS (ESI) calcd for $C_{28}H_{25}ClN_8O_3$ $[M+1]^+$ 557.1738, found 557.1756.

4.1.4.6. (E)-N'-(4-((1-(3-((7-chloroquinolin-4-yl)amino)propyl)-1H-1,2,3-triazol-4-yl)methoxy)-3-methoxybenzylidene)isonicotinohydrazide(16f)

Yield 71%, pale white solid, MP = 132-134ºC, ^1H NMR (400 MHz, DMSO-d_6)δ: 2.29-2.32 (m, 2H, -CH_2), 3.81 (s, 3H, -OCH_3), 4.59 (t, *J* = 6.0 Hz, 2H, -CH_2), 5.20 (s, 2H, -OCH_2), 6.74 (d, *J* = 5.0 Hz, 1H, Ar-H), 7.20-7.23 (m, 2H, Ar-H), 7.45 (s, 1H, Ar-H), 7.65 (d, *J* = 8.3 Hz, 1H, Ar-H), 7.76-7.81 (m, 5H, $2H^b$ +3Ar-H), 8.29 (s, 1H, triazole-H), 8.37 (s, 1H, -CH=N), 8.78 (d, *J* = 5.1 Hz, 2H, H^a), 12.02 (s, 1H, -NH (exchangeable with D_2O)). ^{13}C NMR (100 MHz, DMSO-d_6)δ: 28.5, 40.9, 47.8, 55.5, 62.3, 109.8, 113.7, 117.7, 120.1, 121.7, 122.4, 125.7, 127.5, 127.9, 128.2, 129.4, 133.2, 140.8, 142.9, 144.1, 148.3, 149.7, 150.8, 152.8, 160.1, 162.4. HRMS (ESI) calcd for $C_{29}H_{27}ClN_8O_3$ $[M+1]^+$ 571.1895, found 571.1845.

4.1.4.7. (E)-N'-(2-(4-((4-(7-chloroquinolin-4-yl)piperazin-1-yl)methyl)-1H-1,2,3-triazol-1-yl)benzylidene)isonicotinohydrazide (16g)

Yield 76%, brown semisolid, ^1H NMR (400 MHz, DMSO-d_6) δ: 2.75 (s, 4H, -CH_2), 3.16 (s, 4H, -CH_2), 3.79 (s, 2H, -CH_2), 6.93 (d, *J* = 4.9 Hz, 1H, Ar-H), 7.43-7.65 (m, 7H, 5Ar-H + $2H^b$), 7.92 (d, *J* = 1.9 Hz, 1H, Ar-H), 7.96 (d, *J* = 9.0 Hz, 1H, Ar-H), 8.19 (s, 1H, triazole-H), 8.51 (s, 1H, -CH=N), 8.64 (d, *J* = 4.8 Hz, 1H, H^a), 8.69 (d, *J* = 3.6 Hz, 1H, H^a), 8.95 (s, 1H, Ar-H), 12.13 (s, 1H, -NH (exchangeable with D_2O)). ^{13}C NMR (100 MHz, DMSO-d_6) δ: 52.2, 52.7, 52.8, 109.1, 121.8, 124.0, 126.2, 126.5, 126.9, 128.5, 129.3, 129.8, 130.6, 131.5, 134.1, 135.2, 143.8, 144.3, 149.1, 150.1, 152.2, 152.7, 156.7, 162.3. HRMS (ESI) calcd for $C_{29}H_{26}ClN_9O$ $[M+1]^+$ 552.1949, found 552.1923.

4.1.4.8. (E)-N'-(4-((1-(7-chloroquinolin-4-yl)-1H-1,2,3-triazol-4-yl)methoxy)benzylidene)nicotinohydrazide (17a)

Yield 76%, pale white solid, MP = 238-241°C, ^{1}H NMR (400 MHz, DMSO- d_6) δ: 5.16 (s, 2H, -OCH_2), 7.15 (d, J = 7.6Hz, 2H, Ar-H), 7.48-7.61 (m, 4H, 3Ar-H+ H^d), 8.01-8.06 (m, 2H, Ar-H), 8.26 (s, 1H, triazole-H), 8.31-8.36 (m, 3H, -CH=N +Ar-H), 8.91-9.09 (m, 3H, H^b +H^c +H^a), 11.97 (s, 1H, -NH (exchangeable with D_2O)). ^{13}C NMR (100 MHz, DMSO-d_6) δ: 61.4, 115.6, 117.6, 120.7, 125.9, 127.5, 127.6, 128.6, 129.5, 129.5, 130.5, 132.3, 135.9, 140.8, 143.8, 144.6, 149.9, 150.0, 152.8, 159.8, 160.2, 163.3. HRMS (ESI) calcd for $C_{25}H_{18}ClN_7O_2$ $[M+1]^+$ 484.1211, found 484.1171.

4.1.4.9. (E)-N'-(4-((1-(7-chloroquinolin-4-yl)-1H-1,2,3-triazol-4-yl)methoxy)-3-methoxybenzylidene)nicotinohydrazide (17b)

Yield 71% , brown solid, MP = 270-272°C, ^{1}H NMR (400 MHz, DMSO-d_6) δ: 3.79 (s, 3H, -OCH_3), 5.32 (s, 2H, -OCH_2), 7.23-7.27(m, 2H, Ar-H), 7.36(s, 1H, H^d), 7.71-7.99 (m, 4H, Ar-H), 8.22-8.35 (m, 4H, triazole-H + CH=N + 2Ar-H), 8.94-9.12 (m, 3H,H^a +H^b +H^c), 11.91 (s, 1H, -NH (exchangeable with D_2O)).^{13}C NMR (100 MHz, DMSO-d_6) δ: 56.2, 62.4, 109.3, 113.9, 121.0, 122.7, 125.7, 126.3, 127.1, 128.0, 138.0, 143.1, 144.0, 144.7, 144.9, 145.4, 148.5, 150.0, 150.3, 150.6, 155.4, 160.0. HRMS (ESI) calcd for $C_{26}H_{20}ClN_7O_3$ $[M+1]^+$ 514.1316, found 514.1367.

4.1.4.10. (E)-N'-(4-((1-(2-((7-chloroquinolin-4-yl)amino)ethyl)-1H-1,2,3-triazol-4-yl)methoxy)benzylidene)nicotinohydrazide (17c)

Yield 72%, light brown solid , MP = 226-228°C, ^{1}H NMR (400 MHz, DMSO-d_6)δ: 3.82 (s, 3H, -CH_2+NH (exchangeable with D_2O)), 4.66 (s, 2H, -CH_2-), 5.13 (s, 2H, -OCH_2), 7.05 (d, J = 7.6Hz, 2H, Ar-H), 7.50-7.64 (m, 4H, 3Ar-H+ H^a), 8.01-8.06 (m, 2H, Ar-H), 8.25-8.36 (m, 5H, triazole-H + -CH=N + H^c+ Ar-H), 8.92-9.01 (m,2H, H^a +H^b), 11.97 (s, 1H, -NH (exchangeable with D_2O)). ^{13}C NMR (100 MHz, DMSO-d_6)δ: 42.7, 48.2, 61.6, 115.3, 116.2, 123.1, 124.3, 125.2, 125.4, 125.6, 128.6, 129.8, 130.2, 132.4, 132.9, 135.1, 135.4, 135.8, 142.1, 148.9, 151.6, 152.9, 159.8, 160.2. HRMS (ESI) calcd for $C_{27}H_{23}ClN_8O_2$ $[M+1]^+$ 527.1632, found 527.1676.

4.1.4.11. (E)-N'-(4-((1-(3-((7-chloroquinolin-4-yl)amino)propyl)-1H-1,2,3-triazol-4-yl)methoxy)benzylidene)nicotinohydrazide (17d)

Yield 70%, pale white solid, MP = 136-138°C, ^{1}H NMR (400 MHz, DMSO-d_6) δ: 2.16-2.21 (m, 2H, -CH_2), 4.21 (t, J = 6.8 Hz, 2H,-CH_2), 5.17 (s, 2H, -OCH_2), 7.10 (d, J = 7.8 Hz, 2H, Ar-H), 7.52-7.68

(m, 4H, 3Ar-H+ H^d), 8.04-8.08 (m, 2H, Ar-H), 8.29-8.38 (m, 5H, triazole-H + -CH=N + H^c+ Ar-H), 8.93-9.01 (m, 2H, H^a +H^b), 12.01 (s, 1H, -NH (exchangeable with D_2O)). ^{13}C NMR (100 MHz, DMSO-d_6) δ: 28.9, 47.9, 49.2, 62.2, 115.8, 116.4, 120.1, 123.4, 124.4, 124.9, 125.1, 125.3, 125.6, 129.8, 132.4, 132.6, 135.1, 135.9, 140.1, 141.9, 142.7, 148.9, 151.9, 152.8, 162.1. HRMS (ESI) calcd for $C_{28}H_{25}ClN_8O_2$ $[M+1]^+$ 541.1789, found 541.1721.

4.1.4.12. (E)-N'-(4-((1-(2-((7-chloroquinolin-4-yl)amino)ethyl)-1H-1,2,3-triazol-4-yl)methoxy)-3-methoxybenzylidene)nicotinohydrazide (17e)

Yield 72%, light brown solid, MP = 194-196^{o}C, ^{1}H NMR (400 MHz, DMSO-d_6) δ: 3.23-2.84 (m, 3H, -CH_2 +-NH (exchangeable with D_2O)), 3.82 (s, 3H, -OCH_3), 4.74 (s, 2H, -CH_2), 5.19 (s, 2H, -OCH_2), 7.21-7.26 (m, 2H, Ar-H), 7.41 (s, 1H, H^d), 7.72-8.10 (m, 4H, Ar-H), 8.27 (s, 1H,triazole-H), 8.32 (m, 3H, triazole-H + CH=N + 2Ar-H), 8.94-9.12 (m, 3H, H^a +H^b +H^c), 11.91 (s, 1H, -NH (exchangeable with D_2O)).^{13}C NMR (100 MHz, DMSO-d_6) δ: 42.6, 47.9, 55.7, 61.9, 100.2, 113.7, 117.8, 123.1, 124.6, 124.8, 125.9, 126.3, 126.4, 127.2, 129.8, 130.4, 134.1, 135.1, 142.6, 148.6, 151.2, 151.7, 152.8, 159.8, 162.1. HRMS (ESI) calcd for $C_{28}H_{25}ClN_8O_3$ $[M+1]^+$ 557.1738, found 557.1778.

4.1.4.13. (E)-N'-(4-((1-(3-((7-chloroquinolin-4-yl)amino)propyl)-1H-1,2,3-triazol-4-yl)methoxy)-3-methoxybenzylidene)nicotinohydrazide (17f)

Yield 78%, brown semisolid, ^{1}H NMR (400 MHz, DMSO- d_6) δ: 2.27-2.31 (m, 2H, -CH_2), 3.83 (s, 3H, -OCH_3), 4.57 (t, J = 6.0 Hz, 2H, -CH_2), 5.21 (s, 2H, -OCH_2), 7.23-7.29 (m, 2H, Ar-H), 7.47 (s, 1H, H^d), 7.73-8.11 (m, 4H, Ar-H), 8.29 (s, 1H, triazole-H), 8.31 (m, 3H, CH=N + 2Ar-H), 8.94-9.10 (m, 3H, H^a +H^b +H^c), 11.97 (s, 1H, -NH (exchangeable with D_2O)). ^{13}C NMR (100 MHz, DMSO-d_6)δ: 28.7, 40.9, 47.8, 56.0, 62.3, 109.8, 113.2, 117.9, 123.4, 124.3, 124.9, 125.8, 126.0, 127.1, 127.3, 129.8, 135.1, 135.6, 142.8, 148.7, 148.9, 149.7, 150.7, 151.8, 152.3, 155.2, 160.2. HRMS (ESI) calcd for $C_{29}H_{27}ClN_8O_3$ $[M+1]^+$ 571.1895, found 571.1834.

4.1.4.14. (E)-N'-(2-(4-((4-(7-chloroquinolin-4-yl)piperazin-1-yl)methyl)-1H-1,2,3-triazol-1-yl)benzylidene)nicotinohydrazide(17g)

Yield 78% , brown semisolid, ^{1}H NMR (400 MHz, DMSO-d_6)δ: 2.76 (s, 4H, -CH_2), 3.14 (s, 4H, -CH_2), 3.81 (s, 2H, -CH_2), 6.97 (d, J = 5.1Hz, 1H, Ar-H), 7.39-7.60 (m, 6H, 5Ar-H + H^d), 7.78 (m,

1H, Ar-H), 8.30 (s, 1H, triazole-H), 8.31-8.35 (m, 2H, Ar-H), 8.38 (s, 1H, -CH=N), 8.91-9.09 (m, 3H, H^a +H^b +H^c), 11.98 (s, 1H, -NH (exchangeable with D_2O)). ^{13}C NMR (100 MHz, DMSO-d_6) δ: 52.1, 52.6, 52.9, 109.1, 123.4, 124.9, 125.2, 125.7, 126.9, 128.7, 129.1, 129.8, 130.4, 131.2, 134.4, 135.0, 135.2, 138.1, 139.4, 145.2, 148.9, 151.8, 152.4, 156.8, 162.4. HRMS (ESI) calcd for $C_{29}H_{26}ClN_9O$ $[M+1]^+$ 552.1949, found 552.1921.

4.1.4.15. (E)-N'-(4-((1-(7-chloroquinolin-4-yl)-1H-1,2,3-triazol-4-yl)methoxy)benzylidene)pyrazine-2-carbohydrazide (18a)

Yield 75%, pale white solid, MP = 235-237°C, ^1H NMR (500 MHz, DMSO-d_6) δ: 5.41 (s, 2H, -OCH_2), 7.23 (d, *J* = 8.3 Hz, 2H, Ar-H), 7.73 (d, *J* = 8.2 Hz, 2H, Ar-H), 7.81 (d, *J* = 9.0 Hz, 1H, Ar-H), 7.89 (d, *J* = 4.0 Hz, 1H, Ar-H), 8.02 (d, *J* = 9.0 Hz, 1H, Ar-H), 8.30 (s, 1H, triazole-H), 8.61 (s, 1H, -CH=N), 8.79 (s, 1H, Ar-H), 8.93 (s, 1H, Ar-H), 9.01 (s, 1H, H^c), 9.17 (d, *J* = 4.0 Hz, 1H, H^b), 9.27 (s, 1H, H^a), 12.19 (s, 1H, -NH (exchangeable with D_2O)). ^{13}C NMR (125 MHz, DMSO-d_6) δ: 61.4, 115.7, 117.6, 120.7, 125.8, 127.5, 127.6, 128.6, 129.4, 129.5, 135.8, 143.7, 143.8, 144.5, 145.2, 148.2, 149.8, 150.0, 152.8, 159.8, 160.2. HRMS (ESI) calcd for $C_{24}H_{17}ClN_8O_2$ $[M+1]^+$ 485.1163, found 485.1121.

4.1.4.16. (E)-N'-(4-((1-(7-chloroquinolin-4-yl)-1H-1,2,3-triazol-4-yl)methoxy)-3-methoxybenzylidene)pyrazine-2-carbohydrazide (18b)

Yield 72% , brown solid , MP = 249-251°C, ^1H NMR (500 MHz, DMSO-d_6) δ: 3.82 (s, 3H, -OCH_3), 5.36 (s, 2H, -OCH_2), 7.27-7.32 (m, 2H, Ar-H), 7.47 (s, 1H, Ar-H), 7.77-7.84 (m, 2H, Ar-H), 7.98 (d, *J* = 8.6 Hz, 1H, Ar-H), 8.26 (s, 1H, triazole-H), 8.53 (s, 1H, -CH=N), 8.78 -8.94 (m, 3H, H^b +H^c +Ar-H), 9.14 (s, 1H, Ar-H), 9.27 (s, 1H, H^a), 12.22 (s, 1H, -NH (exchangeable with D_2O)). ^{13}C NMR (125 MHz, DMSO-d_6) δ: 55.9, 61.7, 109.2, 113.8, 117.5, 120.7, 122.6, 125.7, 127.6, 127.9, 128.4, 129.5, 135.9, 140.7, 143.7, 144.3, 148.2, 149.7, 149.8, 149.9, 150.5, 152.8, 160.0. HRMS (ESI) calcd for $C_{25}H_{19}ClN_8O_3$ $[M+1]^+$ 515.1269, found 515.1213.

4.1.4.17. (E)-N'-(4-((1-(2-((7-chloroquinolin-4-yl)amino)ethyl)-1H-1,2,3-triazol-4-yl)methoxy)benzylidene)pyrazine-2-carbohydrazide (18c)

Yield 74%, pale white solid, MP = 231-23 °C, ^1H NMR (500 MHz, DMSO-d_6) δ: 3.85 (d, *J* = 4.3 Hz, 2H, -CH_2), 4.70 (s, 2H, -CH_2), 5.19 (s, 2H, -OCH_2), 6.95 (s, 1H, -NH (exchangeable with D_2O)), 7.11

(d, *J* = 8.2 Hz, 2H, Ar-H), 7.51 (d, *J* = 8.8 Hz, 1H, Ar-H), 7.66-7.79 (m, 4H, Ar-H), 8.26-8.29 (m, 2H, triazole-H, Ar-H), 8.58 (s, 1H, -CH=N), 8.79-8.93 (m, 3H, H^b +H^c +Ar-H), 9.27 (s, 1H, H^a), 12.17 (s, 1H, -NH (exchangeable with D_2O)). ^{13}C NMR (125 MHz, DMSO-d_6) δ: 42.9, 48.3, 61.6, 115.5, 124.7, 125.3, 125.6, 127.4, 129.3, 132.2, 132.7, 134.6, 142.8, 143.0, 143.7, 144.5, 145.2, 148.2, 150.1, 159.7, 160.2. HRMS (ESI) calcd for $C_{26}H_{22}ClN_9O_2$ $[M+1]^+$ 528.1585, found 528.1543

4.1.4.18. (E)-N'-(4-((1-(3-((7-chloroquinolin-4-yl)amino)propyl)-1H-1,2,3-triazol-4-yl)methoxy)benzylidene)pyrazine-2-carbohydrazide (18d)

Yield 74%, pale white solid, MP = 144-147°C, ^{1}H NMR (400 MHz, DMSO-d_6) δ: 2.22 (t, *J* = 5.5 Hz, 2H, -CH_2), 3.36-3.37 (m, 2H, -CH_2), 4.50 (t, *J* = 6.7 Hz, 2H, -CH_2), 5.15 (s, 2H, -OCH_2), 7.08 (d, *J* = 8.6 Hz, 2H, Ar-H), 7.55 (d, *J* = 8.9 Hz, 1H, Ar-H), 7.64 (d, *J* = 8.5 Hz, 3H, Ar-H), 8.27 (s, 1H, triazole-H), 8.29-8.39 (m, 2H, Ar-H), 8.51-8.73 (m, 3H, H^c+Ar-H), 8.87 (s, 1H, H^b), 9.21 (s, 1H, H^a), 12.13 (s, 1H, -NH (exchangeable with D_2O)). ^{13}C NMR (125 MHz, DMSO-d_6) δ: 28.7, 40.5, 47.8, 61.6, 115.5, 125.3, 125.5, 125.9, 127.4, 129.4, 129.6, 132.2, 136.0, 142.8, 143.8, 144.4, 145.1, 148.2, 150.1, 152.9, 159.8, 160.2. HRMS (ESI) calcd for $C_{27}H_{24}ClN_9O_2$ $[M+1]^+$ 542.1741, found 542.1782.

4.1.4.19. (E)-N'-(4-((1-(2-((7-chloroquinolin-4-yl)amino)ethyl)-1H-1,2,3-triazol-4-yl)methoxy)-3-methoxybenzylidene)pyrazine-2-carbohydrazide (18e)

Yield 75%, pale white solid, MP = 234-237°C, ^{1}H NMR (500 MHz, DMSO-d_6) δ: 3.23-3.29 (m, 3H, -CH_2 +-NH (exchangeable with D_2O)), 3.81 (s, 3H, -OCH_3), 4.73 (s, 2H, -CH_2), 5.18 (s, 2H, -OCH_2), 6.81 (d, *J* = 5.1 Hz, 1H, Ar-H), 7.24 (dd, *J* = 18.4, 6.5 Hz, 2H, Ar-H), 7.39 (s, 1H, Ar-H), 7.71 (d, *J* = 8.5 Hz, 1H, Ar-H), 8.21 (s, 1H, Ar-H), 8.35 (s, 1H, triazole-H), 8.51 (s, 1H, -CH=N), 8.54 (d, *J* = 8.6 Hz, 1H, Ar-H), 8.79-8.86 (m, 3H, H^b +H^c +Ar-H), 9.27 (s, 1H, H^a), 12.19 (s, 1H, NH (exchangeable with D_2O)). ^{13}C NMR (125 MHz, DMSO-d_6) δ: 42.9, 48.3, 55.8, 61.6, 109.2, 113.8, 122.3, 125.3, 126.0, 126.9, 127.4, 137.8, 142.9, 143.7, 144.3, 145.1, 148.5, 149.8, 150.1, 150.3, 155.9, 160.1. HRMS (ESI) calcd for $C_{27}H_{24}ClN_9O_3$ $[M+1]^+$ 558.1691, found 558.1635.

4.1.4.20. (E)-N'-(4-((1-(3-((7-chloroquinolin-4-yl)amino)propyl)-1H-1,2,3-triazol-4-yl)methoxy)-3-methoxybenzylidene)pyrazine-2-carbohydrazide (18f)

Yield 76%, pale white solid, MP = 146-148°C, ^{1}H NMR (500 MHz, DMSO-d_6) δ: 2.28-2.30 (m, 2H, -CH_2), 3.52-3.54 (m, 3H, -CH_2+-NH (exchangeable with D_2O)), 3.82 (s, 3H, -OCH_3), 4.57 (t, *J* = 5.9

Hz, 2H, -CH_2), 5.18 (s, 2H, -OCH_2), 6.78 (d, *J* = 5.2 Hz, 1H, Ar-H), 7.22 (dd, *J* = 18.0, 8.0 Hz, 2H, Ar-H), 7.37 (s, 1H, Ar-H), 7.73 (d, *J* = 8.6 Hz, 1H, Ar-H), 8.00 (s, 1H, Ar-H), 8.34 (s, 1H, triazole-H), 8.55 (s, 1H, -CH=N), 8.59 (d, *J* = 8.8 Hz, 1H, Ar-H), 8.79-8.93 (m, 3H, H^b +H^c +Ar-H), 9.26 (s, 1H, H^a), 12.18 (s, 1H, -NH (exchangeable with D_2O)). ^{13}C NMR (125 MHz, DMSO-d_6) δ: 28.6, 40.8, 47.7, 55.9, 62.1, 109.1, 113.6, 122.4, 125.5, 126.0, 126.9, 127.7, 137.7, 142.8, 143.8, 144.5, 145.2, 148.2, 149.7, 150.0, 150.3, 155.1, 159.8. HRMS (ESI) calcd for $C_{28}H_{26}ClN_9O_3$ $[M+1]^+$ 572.1847, found 572.1872.

4.1.4.21. (E)-N'-(2-(4-((4-(7-chloroquinolin-4-yl)piperazin-1-yl)methyl)-1H-1,2,3-triazol-1-yl)benzylidene)pyrazine-2-carbohydrazide (18g)

Yield 73%, brown semisolid, ^{1}H NMR (400 MHz, DMSO-d_6) δ: 2.76 (s, 4H, -CH_2), 3.16 (s, 4H, -CH_2), 3.80 (s, 2H, -CH_2), 6.93 (d, *J* = 5.0 Hz, 1H, Ar-H), 7.47 (dd, *J* = 9.0 Hz, 2.0 Hz, 1H, Ar-H), 7.55-7.64 (m, 3H, Ar-H), 7.91 (d, *J* = 1.7 Hz, 1H, Ar-H), 7.96 (d, *J* = 9.0 Hz, 1H, Ar-H), 8.16-8.18 (m, 1H, Ar-H), 8.41 (s, 1H, triazole-H), 8.49 (s, 1H, -CH=N), 8.64 (s, 2H, H^c+Ar-H), 8.82 (d, *J* = 2.2 Hz, 1H, H^b), 9.19 (s, 1H, H^a), 12.47 (s, 1H, -NH (exchangeable with D_2O)). ^{13}C NMR (100 MHz, DMSO-d_6) δ: 52.1, 52.7, 52.9, 109.2, 121.9, 124.3, 126.1, 126.6, 126.8, 128.6, 129.8, 130.7, 131.6, 134.2, 135.3, 137.7, 143.9, 144.2, 149.4, 150.2, 152.3, 152.8, 156.9, 162.1. HRMS (ESI) calcd for $C_{28}H_{25}ClN_{10}O$ $[M+1]^+$ 553.1901, found 553.1934.

4.2. Strains, plasmids, and culture conditions

The pantothenate-auxotrophic *M. tuberculosis* $mc^2$6230 strain [52] was grown in Middlebrook 7H9 broth supplemented with 10% oleic-albumin-dextrose-catalase enrichment (OADC), 0.025% tyloxapol and 109 µM pantothenic acid or Middlebrook7H10 agar supplemented with OADC and with 109 µM pantothenic acid at 37 °C without agitation. Recombinant strains carrying pMV261-*inhA* [38] were grown in a 7H9 broth medium containing 25 µg/mL kanamycin or on Middlebrook 7H10 agar supplemented with 10% OADC containing 25 µg/mL kanamycin at 37 °C for either 2 weeks. *M. marinum* M strain [53] and *M. abscessus* $CIP104536^T$ [54] were grown in 7H9 broth supplemented with OADC enrichment and 0.025% tyloxapol.

4.3. Drug susceptibility testing

MIC was defined as the lowest concentration of compound inhibiting 99% of bacterial growth, at which no change in turbidity was observed and performed in 7H9 broth supplemented with 10% OADC, 0.025% tyloxapol at 37 °C without agitation (for *Mtb* and *M. marinum*) and in CaMHB for *M. abscessus* according to the CLSI guidelines [55]. For *Mtb* mc^26230, 109 µM pantothenic acid was added to all experiments. MIC determination was done using the broth dilution method. Briefly, a log-phase (OD_{600} ~ 1) culture was diluted to an OD_{600} = 0.05 (*Mtb*) in 7H9 medium or with an inoculum containing 5.10^6 CFU/mL (*M. marinum* and *M. abscessus*) and deposited in 96-well plates. Compounds were then directly added (in general 4 µL/well of a 10 mg/mL stock solution) to the first-row wells. Serial 2-fold dilutions were then completed starting from the first row. Plates were wrapped in parafilm and were then placed in a 37 °C incubator and observed after 7 days for *Mtb* or at 30 °C and observed after 6 days for *M. marinum* and 4 days for *M. abscessus*. Control wells included DMSO as vehicle control, in which bacterial growth was not inhibited (as for untreated wells). INH was included as a reference drug.

4.4. Kill kinetics

Kill kinetic experiments were completed as previously described [56, 57]. Briefly, *Mtb* mc^26230 was grown to log-phase (OD_{600} ~ 1), diluted to an OD_{600} = 0.05 and deposited into all wells of a 96-well microtiter plate. Increasing concentrations of compounds **16a-g** and INH (positive control) were added to each well corresponding to 1x, 5x, and 20x the respective MIC values. DMSO was included as a negative control and was added to the respective wells at the highest volume used in the experiment. Plates were sealed with parafilm and left to incubate at 37 °C until required. At the designated time points, 20 µL of each required well was serially diluted in sterile PBS and plated on 7H10 agar medium supplemented with 10% OADC and 109 µM pantothenic acid. Plates were incubated at 37 °C for 3 weeks until visible colonies formed and were enumerated by visual inspection.

4.5. Cell culture and cytotoxicity assay

Vero kidney epithelial cells (ATCC® CCL-81) and human THP-1 monocytes were cultured in RPMI 1640 (Life Technologies) supplemented with 10% foetal calf serum (Sigma-Aldrich) and incubated at 37 °C and 5% CO_2. Once the desired confluency was achieved, cells were detached from the flask surface using trypsin (ThermoFisher) before adding 4mL of culture medium and enumerated in a

Malassez counting chamber. Cell density was adjusted to 2 x 10^4 cells/well in a 96-well microtiter plate and left to adhere overnight at 37 °C and 5% CO_2. Monocytes were differentiated into macrophages in the presence of 20 ng/mL Phorbol Myristate Acetate (PMA) in a 96-well flat-bottom tissue culture plate (1 x 10^5 cells/well) and incubated for 48 hrs at 37 °C and 5% CO_2. Serial dilutions of the test compounds (ranging from 100 µg/mL to 0.78 µg/mL) were added to the cells, which were further incubated at 37 °C and 5% CO_2 for 24 hrs after which 10% (vol/vol) resazurin dye was added to each well and left to incubate for 4 hrs at 37 °C and 5% CO_2. INH and RFB were included as reference drugs. Data were acquired using a fluorescent plate reader (excitation 540 nm, emission 590 nm).

4.6. Generation of spontaneous mutants and genotyping

Spontaneous *Mtb* mutants resistant to compounds **16d, 16g,** and **16f** were selected by diluting and plating mid-log phase cultures at ~1 x 10^8 CFU/mL on 7H10 agar medium supplemented with OADC, pantothenic acid, and 5x or 20x the respective MIC of the compounds. The frequency of spontaneous resistant mutants was enumerated by visual inspection of the colonies. One individual colony growing on each compound was picked was subsequently grown in 7H9 medium supplemented with OADC, tyloxapol and pantothenic acid. The degree of resistance (and cross-resistance) to compounds **16d, 16g,** and **16f** and INH was evaluated by MIC determination. The *katG* gene in the various resistant mutants was PCR amplified using Q5 high fidelity polymerase (NEB), and the resulting products were purified using a PCR clean-up system (Macherey-Nagel) prior to sequencing using the specific oligonucleotides: 5'-cggtcttgcggggttatcgc-3'; 5'-gaagctctcatgggcggacc-3'; 5'-cctctcgctgcgggtggatc-3' and 5'-aactacctcggaaagggcaacc-3'.

4.7. Whole-genome sequencing

DNA was extracted using NucleoBond AXG 100 DNA kit (Macherey-Nagel, Germany) according to the manufacturer's instructions. DNA was quantified using Qubit™ dsDNA BR Assay Kit and Qubit™ 4 fluorometer (Invitrogen, Thermo Fischer Scientific). Library preparation and Illumina sequencing was performed by Novogene (Cambridge, UK) on IlluminaNovaSeq platform (2x150bp). The short-read data were first trimmed using fastp v0.23.2 [58], based on a Phred scale base quality threshold of Q30 and removing reads of less than 21 bp. Kraken2 v2.0.9-beta [59] with the bacteria database was used to perform taxonomic identification at the read level in order to check for potential

contamination. All reads assigned to the Mycobacteriaceae family were extracted and then assembled using SPAdes v3.15.3 [60] with the "--careful" option. Reads were mapped to H37Rv reference genome using Burrow-Wheeler Aligner (BWA) mem (v0.7.17-r1188) (http://arxiv.org/abs/1303.3997).

4.8. Fatty acid and mycolic acid analysis

To appreciate the drug-induced changes in the lipid profile, *Mtb* mc^{2}6230 cultures were exposed to increasing drug concentrations of INH or **16g** for 15 hrs prior to metabolic labeling in the presence of 1 μCi/mL of [2-^{14}C]acetate (59 mCi/mmol, Perkin Elmer) for an additional 7 hrs at 37 °C. Extraction of total mycolic acids was carried out as previously reported [61]. Briefly, cell pellets were washed and treated with 15% tetrabutylammonium hydroxide (TBAH) at 100 °C overnight. Fatty acids and mycolic acids were methyl-esterified and extracted in diethyl ether. Extracts were dried and resuspended in dichloromethane for application to a silica-coated plate for thin-layer chromatography (TLC). Fatty acid methyl esters (FAMEs) and mycolic acid methyl esters (MAMEs) were developed twice on normal phase TLC in hexane/ethyl acetate (19/1, v/v). The [^{14}C]-labeled FAME and MAME contents were analyzed using an Amersham Typhoon imaging system.

4.9. Statistical analyses

Statistical analyses were performed on Prism 5.0 (Graphpad) and detailed for each figure legend. *p<0.05; **p<0.01; ***p<0.001.

Author contributions

MA, BS, FRB, CC, TC conducted experiments and analyzed the data. FB, VK and LK analyzed the data. MA, BS, VK, and LK wrote the manuscript. VK and LK conceived, supervised the project, and acquired funding.

Declaration of competing interest

The funders had no role in study design, data collection, interpretation, or the decision to submit the work for publication. The authors have no conflict of interest to declare.

Acknowledgments

The authors wish to thank A. Speer for the generous gift of pSMT3-*katG*, the Ministère de l'Enseignement Supérieur, de la Recherche et de l'Innovation for funding MA. VK thanks Council of Scientific and Industrial Research (CSIR) for providing financial support (grant no. 02(0400)/21/EMR-II). B.S. acknowledges the Council of Scientific and Industrial Research, New Delhi, India, for providing CSIR-SRF fellowship (CSIR Ref No. 09/254(0257)/2016-EMR-I).

References

[1] 2020 WHO., Global tuberculosis report 2020. Geneva: World Health Organization, 2020. https://www.who.int/tb/publications/global_report/en/, (n.d.).

[2] WHO, Impact of the covid-19 pandemic on TB detection and mortality in 2020. https://www.who.int/publications/m/item/impact-of-the-covid-19-pandemic-on-tb-detection-and-mortality-in-2020, (2020). https://www.who.int/publications/m/item/impact-of-the-covid-19-pandemic-on-tb-detection-and-mortality-in-2020 (accessed February 18, 2015).

[3] S.C. Duffy, S. Srinivasan, M.A. Schilling, T. Stuber, S.N. Danchuk, J.S. Michael, M. Venkatesan, N. Bansal, S. Maan, N. Jindal, D. Chaudhary, P. Dandapat, R. Katani, S. Chothe, M. Veerasami, S. Robbe-Austerman, N. Juleff, V. Kapur, M.A. Behr, Reconsidering *Mycobacterium bovis* as a proxy for zoonotic tuberculosis: a molecular epidemiological surveillance study, Lancet Microbe. 1 (2020) e66–e73. https://doi.org/10.1016/S2666-5247(20)30038-0.

[4] GBD 2019 Tuberculosis Collaborators, Global, regional, and national sex differences in the global burden of tuberculosis by HIV status, 1990-2019: results from the Global Burden of Disease Study 2019, Lancet Infect. Dis. (2021) S1473-3099(21)00449–7. https://doi.org/10.1016/S1473-3099(21)00449-7.

[5] K. Dheda, T. Gumbo, G. Maartens, K.E. Dooley, R. McNerney, M. Murray, J. Furin, E.A. Nardell, L. London, E. Lessem, G. Theron, P. van Helden, S. Niemann, M. Merker, D. Dowdy, A. Van Rie, G.K.H. Siu, J.G. Pasipanodya, C. Rodrigues, T.G. Clark, F.A. Sirgel, A. Esmail, H.-H. Lin, S.R. Atre, H.S. Schaaf, K.C. Chang, C. Lange, P. Nahid, Z.F. Udwadia, C.R. Horsburgh, G.J. Churchyard, D. Menzies, A.C. Hesseling, E. Nuermberger, H. McIlleron, K.P. Fennelly, E. Goemaere, E. Jaramillo, M. Low, C.M. Jara, N. Padayatchi, R.M. Warren, The epidemiology, pathogenesis, transmission, diagnosis, and management of multidrug-resistant, extensively drug-resistant, and incurable tuberculosis, Lancet Respir. Med. (2017) S2213-2600(17)30079–6. https://doi.org/10.1016/S2213-2600(17)30079-6.

[6] S. Huszár, K. Chibale, V. Singh, The quest for the holy grail: new antitubercular chemical entities, targets and strategies, Drug Discov. Today. 25 (2020) 772–780. https://doi.org/10.1016/j.drudis.2020.02.003.

[7] A. Koul, E. Arnoult, N. Lounis, J. Guillemont, K. Andries, The challenge of new drug discovery for tuberculosis, Nature. 469 (2011) 483–490. https://doi.org/10.1038/nature09657.

[8] J. Harrison, J.A.G. Cox, Changing the Rules of TB-Drug Discovery, J. Med. Chem. 62 (2019) 10583–10585. https://doi.org/10.1021/acs.jmedchem.9b01716.

[9] S. Wellington, D.T. Hung, The expanding diversity of *Mycobacterium tuberculosis* drug targets, ACS Infect. Dis. 4 (2018) 696–714. https://doi.org/10.1021/acsinfecdis.7b00255.

[10] Q. An, C. Li, Y. Chen, Y. Deng, T. Yang, Y. Luo, Repurposed drug candidates for antituberculosis therapy, Eur. J. Med. Chem. 192 (2020) 112175. https://doi.org/10.1016/j.ejmech.2020.112175.
[11] B.S. Matada, R. Pattanashettar, N.G. Yernale, A comprehensive review on the biological interest of quinoline and its derivatives, Bioorg. Med. Chem. 32 (2021) 115973. https://doi.org/10.1016/j.bmc.2020.115973.
[12] A. Koul, N. Dendouga, K. Vergauwen, B. Molenberghs, L. Vranckx, R. Willebrords, Z. Ristic, H. Lill, I. Dorange, J. Guillemont, D. Bald, K. Andries, Diarylquinolines target subunit c of mycobacterial ATP synthase, Nat. Chem. Biol. 3 (2007) 323–324. https://doi.org/10.1038/nchembio884.
[13] A.K. Kakkar, N. Dahiya, Bedaquiline for the treatment of resistant tuberculosis: promises and pitfalls, Tuberculosis (Edinb). 94 (2014) 357–362. https://doi.org/10.1016/j.tube.2014.04.001.
[14] T.G. Shruthi, S. Eswaran, P. Shivarudraiah, S. Narayanan, S. Subramanian, Synthesis, antituberculosis studies and biological evaluation of new quinoline derivatives carrying 1,2,4-oxadiazole moiety, Bioorg. Med. Chem. Lett. 29 (2019) 97–102. https://doi.org/10.1016/j.bmcl.2018.11.002.
[15] A. Banerjee, E. Dubnau, A. Quemard, V. Balasubramanian, K.S. Um, T. Wilson, D. Collins, G. de Lisle, W.R. Jacobs, *inhA*, a gene encoding a target for isoniazid and ethionamide in *Mycobacterium tuberculosis*, Science. 263 (1994) 227–230. https://doi.org/10.1126/science.8284673.
[16] A. Bhatt, V. Molle, G.S. Besra, W.R. Jacobs, L. Kremer, The *Mycobacterium tuberculosis* FAS-II condensing enzymes: their role in mycolic acid biosynthesis, acid-fastness, pathogenesis and in future drug development, Mol. Microbiol. 64 (2007) 1442–1454. https://doi.org/10.1111/j.1365-2958.2007.05761.x.
[17] C. Vilchèze, H.R. Morbidoni, T.R. Weisbrod, H. Iwamoto, M. Kuo, J.C. Sacchettini, W.R. Jacobs, Inactivation of the *inhA*-encoded fatty acid synthase II (FASII) enoyl-acyl carrier protein reductase induces accumulation of the FASI end products and cell lysis of *Mycobacterium smegmatis*, J. Bacteriol. 182 (2000) 4059–4067. https://doi.org/10.1128/jb.182.14.4059-4067.2000.
[18] K. Johnsson, W.A. Froland, P.G. Schultz, Overexpression, purification, and characterization of the catalase-peroxidase KatG from *Mycobacterium tuberculosis*, J. Biol. Chem. 272 (1997) 2834–2840. https://doi.org/10.1074/jbc.272.5.2834.
[19] Y. Zhang, B. Heym, B. Allen, D. Young, S. Cole, The catalase-peroxidase gene and isoniazid resistance of *Mycobacterium tuberculosis*, Nature. 358 (1992) 591–593. https://doi.org/10.1038/358591a0.
[20] D.A. Rozwarski, Modification of the NADH of the isoniazid target (InhA) from *Mycobacterium tuberculosis*, Science. 279 (1998) 98–102. https://doi.org/10.1126/science.279.5347.98.
[21] M. Wilming, K. Johnsson, Spontaneous formation of the bioactive form of the tuberculosis drug isoniazid, Angew. Chem. Int. Ed. Engl. 38 (1999) 2588–2590. https://doi.org/10.1002/(sici)1521-3773(19990903)38:17<2588::aid-anie2588>3.0.co;2-8.
[22] R. Rawat, A. Whitty, P.J. Tonge, The isoniazid-NAD adduct is a slow, tight-binding inhibitor of InhA, the *Mycobacterium tuberculosis* enoyl reductase: adduct affinity and drug resistance, Proc. Natl. Acad. Sci. USA. 100 (2003) 13881–13886. https://doi.org/10.1073/pnas.2235848100.
[23] C. Vilchèze, F. Wang, M. Arai, M.H. Hazbón, R. Colangeli, L. Kremer, T.R. Weisbrod, D. Alland, J.C. Sacchettini, W.R. Jacobs, Transfer of a point mutation in *Mycobacterium*

tuberculosis inhA resolves the target of isoniazid, Nat. Med. 12 (2006) 1027–1029. https://doi.org/10.1038/nm1466.
[24] M. Nguyen, A. Quémard, S. Broussy, J. Bernadou, B. Meunier, Mn(III) pyrophosphate as an efficient tool for studying the mode of action of isoniazid on the InhA protein of *Mycobacterium tuberculosis*, Antimicrob. Agents Chemother. 46 (2002) 2137–2144. https://doi.org/10.1128/aac.46.7.2137-2144.2002.
[25] A.N. Unissa, S. Subbian, L.E. Hanna, N. Selvakumar, Overview on mechanisms of isoniazid action and resistance in *Mycobacterium tuberculosis*, Infect. Gen. Evol. 45 (2016) 474–492. https://doi.org/10.1016/j.meegid.2016.09.004.
[26] M. Seifert, D. Catanzaro, A. Catanzaro, T.C. Rodwell, Genetic mutations associated with isoniazid resistance in *Mycobacterium tuberculosis*: a systematic review, PLoS One. 10 (2015) e0119628. https://doi.org/10.1371/journal.pone.0119628.
[27] S.R. Khan, Y. Manialawy, A.G. Siraki, Isoniazid and host immune system interactions: A proposal for a novel comprehensive mode of action, Br. J. Pharmacol. 176 (2019) 4599–4608. https://doi.org/10.1111/bph.14867.
[28] M.C. Kjellsson, L.E. Via, A. Goh, D. Weiner, K.M. Low, S. Kern, G. Pillai, C.E. Barry, V. Dartois, Pharmacokinetic evaluation of the penetration of antituberculosis agents in rabbit pulmonary lesions, Antimicrob. Agents Chemother. 56 (2012) 446–457. https://doi.org/10.1128/AAC.05208-11.
[29] C.F. de Faria, T. Moreira, P. Lopes, H. Costa, J.R. Krewall, C.M. Barton, S. Santos, D. Goodwin, D. Machado, M. Viveiros, M. Machuqueiro, F. Martins, Designing new antitubercular isoniazid derivatives with improved reactivity and membrane trafficking abilities, Biomed. Pharmacother. 144 (2021) 112362. https://doi.org/10.1016/j.biopha.2021.112362.
[30] M.J. Hearn, M.H. Cynamon, M.F. Chen, R. Coppins, J. Davis, H. Joo-On Kang, A. Noble, B. Tu-Sekine, M.S. Terrot, D. Trombino, M. Thai, E.R. Webster, R. Wilson, Preparation and antitubercular activities *in vitro* and *in vivo* of novel Schiff bases of isoniazid, Eur. J. Med. Chem. 44 (2009) 4169–4178. https://doi.org/10.1016/j.ejmech.2009.05.009.
[31] A. Rani, M.D. Johansen, F. Roquet-Banères, L. Kremer, P. Awolade, O. Ebenezer, P. Singh, Sumanjit, V. Kumar, Design and synthesis of 4-Aminoquinoline-isoindoline-dione-isoniazid triads as potential anti-mycobacterials, Bioorg. Med. Chem. Lett. 30 (2020) 127576. https://doi.org/10.1016/j.bmcl.2020.127576.
[32] M.D. Johansen, Shalini, S. Kumar, C. Raynaud, D.H. Quan, W.J. Britton, P.M. Hansbro, V. Kumar, L. Kremer, Biological and biochemical evaluation of isatin-isoniazid hybrids as bactericidal candidates against *Mycobacterium tuberculosis*, Antimicrob. Agents Chemother. 65 (2021) e0001121. https://doi.org/10.1128/AAC.00011-21.
[33] B. Zhou, Y. He, X. Zhang, J. Xu, Y. Luo, Y. Wang, S.G. Franzblau, Z. Yang, R.J. Chan, Y. Liu, J. Zheng, Z.-Y. Zhang, Targeting mycobacterium protein tyrosine phosphatase B for antituberculosis agents, Proc. Natl. Acad. Sci. USA. 107 (2010) 4573–4578. https://doi.org/10.1073/pnas.0909133107.
[34] B. Sharma, S. Kaur, J. Legac, P.J. Rosenthal, V. Kumar, Synthesis, anti-plasmodial and cytotoxic evaluation of 1H-1,2,3-triazole/acyl hydrazide integrated tetrahydro-β-carboline-4-aminoquinoline conjugates, Bioorg. Med. Chem. Lett. 30 (2020) 126810. https://doi.org/10.1016/j.bmcl.2019.126810.
[35] A. Singh, J. Gut, P.J. Rosenthal, V. Kumar, 4-Aminoquinoline-ferrocenyl-chalcone conjugates: Synthesis and anti-plasmodial evaluation, Eur. J. Med. Chem. 125 (2017) 269–277. https://doi.org/10.1016/j.ejmech.2016.09.044.

[36] P. Tenbrick, M. Beer, K. Beer, Treatment of biopsy and culture negative *Mycobacterium marinum*: diagnostic and therapeutic considerations, J. Drugs Dermatol. 13 (2014) 204–206.
[37] Shalini, A. Viljoen, L. Kremer, V. Kumar, Alkylated/aminated nitroimidazoles and nitroimidazole-7-chloroquinoline conjugates: Synthesis and anti-mycobacterial evaluation, Bioorg. Med. Chem. Lett. 28 (2018) 1309–1312. https://doi.org/10.1016/j.bmcl.2018.03.021.
[38] M.H. Larsen, C. Vilchèze, L. Kremer, G.S. Besra, L. Parsons, M. Salfinger, L. Heifets, M.H. Hazbon, D. Alland, J.C. Sacchettini, W.R. Jacobs, Overexpression of *inhA*, but not *kasA*, confers resistance to isoniazid and ethionamide in *Mycobacterium smegmatis, M. bovis* BCG and *M. tuberculosis*, Mol. Microbiol. 46 (2002) 453–466. https://doi.org/10.1046/j.1365-2958.2002.03162.x.
[39] C.K. Stover, V.F. de la Cruz, T.R. Fuerst, J.E. Burlein, L.A. Benson, L.T. Bennett, G.P. Bansal, J.F. Young, M.H. Lee, G.F. Hatfull, New use of BCG for recombinant vaccines, Nature. 351 (1991) 456–460. https://doi.org/10.1038/351456a0.
[40] L. Kremer, J.D. Douglas, A.R. Baulard, C. Morehouse, M.R. Guy, D. Alland, L.G. Dover, J.H. Lakey, W.R. Jacobs, P.J. Brennan, D.E. Minnikin, G.S. Besra, Thiolactomycin and related analogues as novel anti-mycobacterial agents targeting KasA and KasB condensing enzymes in *Mycobacterium tuberculosis*, J. Biol. Chem. 275 (2000) 16857–16864. https://doi.org/10.1074/jbc.M000569200.
[41] S. Ramaswamy, J.M. Musser, Molecular genetic basis of antimicrobial agent resistance in *Mycobacterium tuberculosis*: 1998 update, Tuber. Lung Dis. 79 (1998) 3–29. https://doi.org/10.1054/tuld.1998.0002.
[42] V.Q.T. Ho, T. Verboom, M.K. Rong, E. Habjan, W. Bitter, A. Speer, Heterologous expression of *ethA* and *katG* in *Mycobacterium marinum* enables the rapid identification of new prodrugs active against *Mycobacterium tuberculosis*, Antimicrob. Agents Chemother. 65 (2021). https://doi.org/10.1128/AAC.01445-20.
[43] C. Vilchèze, W.R. Jacobs, The mechanism of isoniazid killing: clarity through the scope of genetics, Annu. Rev. Microbiol. 61 (2007) 35–50. https://doi.org/10.1146/annurev.micro.61.111606.122346.
[44] K. Rožman, I. Sosič, R. Fernandez, R.J. Young, A. Mendoza, S. Gobec, L. Encinas, A new 'golden age' for the antitubercular target InhA, Drug Discov. Today. 22 (2017) 492–502. https://doi.org/10.1016/j.drudis.2016.09.009.
[45] C. Vilchèze, A.D. Baughn, J. Tufariello, L.W. Leung, M. Kuo, C.F. Basler, D. Alland, J.C. Sacchettini, J.S. Freundlich, W.R. Jacobs, Novel inhibitors of InhA efficiently kill *Mycobacterium tuberculosis* under aerobic and anaerobic conditions, Antimicrob Agents Chemother. 55 (2011) 3889–3898. https://doi.org/10.1128/AAC.00266-11.
[46] B. Inturi, G.V. Pujar, M.N. Purohit, Recent advances and structural features of enoyl-ACP reductase inhibitors of *Mycobacterium tuberculosis*, Arch. Pharm. (Weinheim). 349 (2016) 817–826. https://doi.org/10.1002/ardp.201600186.
[47] L. Flint, A. Korkegian, T. Parish, InhA inhibitors have activity against non-replicating *Mycobacterium tuberculosis*, PLoS One. 15 (2020) e0239354. https://doi.org/10.1371/journal.pone.0239354.
[48] T. Armstrong, M. Lamont, A. Lanne, L.J. Alderwick, N.R. Thomas, Inhibition of *Mycobacterium tuberculosis* InhA: Design, synthesis and evaluation of new di-triclosan derivatives, Bioorg. Med. Chem. 28 (2020) 115744. https://doi.org/10.1016/j.bmc.2020.115744.

[49] A. Gagliardi, P. Selchow, S. Luthra, D. Schäfle, B. Schulthess, P. Sander, KatG as counterselection marker for nontuberculous mycobacteria, Antimicrob. Agents Chemother. 64 (2020) e02508-19, /aac/64/5/AAC.02508-19.atom. https://doi.org/10.1128/AAC.02508-19.
[50] F. Maruri, T.R. Sterling, A.W. Kaiga, A. Blackman, Y.F. van der Heijden, C. Mayer, E. Cambau, A. Aubry, A systematic review of gyrase mutations associated with fluoroquinolone-resistant *Mycobacterium tuberculosis* and a proposed gyrase numbering system, J. Antimicrob. Chemother. 67 (2012) 819–831. https://doi.org/10.1093/jac/dkr566.
[51] K. Andries, P. Verhasselt, J. Guillemont, H.W.H. Göhlmann, J.-M. Neefs, H. Winkler, J. Van Gestel, P. Timmerman, M. Zhu, E. Lee, P. Williams, D. de Chaffoy, E. Huitric, S. Hoffner, E. Cambau, C. Truffot-Pernot, N. Lounis, V. Jarlier, A diarylquinoline drug active on the ATP synthase of *Mycobacterium tuberculosis*, Science. 307 (2005) 223–227. https://doi.org/10.1126/science.1106753.
[52] V.K. Sambandamurthy, S.C. Derrick, T. Hsu, B. Chen, M.H. Larsen, K.V. Jalapathy, M. Chen, J. Kim, S.A. Porcelli, J. Chan, S.L. Morris, W.R. Jacobs, *Mycobacterium tuberculosis* DeltaRD1 DeltapanCD: a safe and limited replicating mutant strain that protects immunocompetent and immunocompromised mice against experimental tuberculosis, Vaccine. 24 (2006) 6309–6320. https://doi.org/10.1016/j.vaccine.2006.05.097.
[53] T.P. Stinear, T. Seemann, P.F. Harrison, G.A. Jenkin, J.K. Davies, P.D.R. Johnson, Z. Abdellah, C. Arrowsmith, T. Chillingworth, C. Churcher, K. Clarke, A. Cronin, P. Davis, I. Goodhead, N. Holroyd, K. Jagels, A. Lord, S. Moule, K. Mungall, H. Norbertczak, M.A. Quail, E. Rabbinowitsch, D. Walker, B. White, S. Whitehead, P.L.C. Small, R. Brosch, L. Ramakrishnan, M.A. Fischbach, J. Parkhill, S.T. Cole, Insights from the complete genome sequence of *Mycobacterium marinum* on the evolution of *Mycobacterium tuberculosis*, Genome Res. 18 (2008) 729–741. https://doi.org/10.1101/gr.075069.107.
[54] F. Ripoll, S. Pasek, C. Schenowitz, C. Dossat, V. Barbe, M. Rottman, E. Macheras, B. Heym, J.-L. Herrmann, M. Daffé, R. Brosch, J.-L. Risler, J.-L. Gaillard, Non mycobacterial virulence genes in the genome of the emerging pathogen *Mycobacterium abscessus*, PLoS One. 4 (2009) e5660. https://doi.org/10.1371/journal.pone.0005660.
[55] G.L. Woods, B.A. Brown-Elliott, P.S. Conville, E.P. Desmond, G.S. Hall, G. Lin, G.E. Pfyffer, J.C. Ridderhof, S.H. Siddiqi, R.J. Wallace, N.G. Warren, F.G. Witebsky, Susceptibility testing of mycobacteria, nocardiae, and other aerobic actinomycetes, 2nd ed., Clinical and Laboratory Standards Institute, Wayne (PA), 2011. http://www.ncbi.nlm.nih.gov/books/NBK544374/ (accessed April 12, 2021).
[56] U.H. Manjunatha, S.P. S. Rao, R.R. Kondreddi, C.G. Noble, L.R. Camacho, B.H. Tan, S.H. Ng, P.S. Ng, N.L. Ma, S.B. Lakshminarayana, M. Herve, S.W. Barnes, W. Yu, K. Kuhen, F. Blasco, D. Beer, J.R. Walker, P.J. Tonge, R. Glynne, P.W. Smith, T.T. Diagana, Direct inhibitors of InhA are active against *Mycobacterium tuberculosis*, Sci. Transl. Med. 7 (2015) 269ra3-269ra3. https://doi.org/10.1126/scitranslmed.3010597.
[57] C. Dupont, Y. Chen, Z. Xu, F. Roquet-Banères, M. Blaise, A.-K. Witt, F. Dubar, C. Biot, Y. Guérardel, F.P. Maurer, S.-S. Chng, L. Kremer, A piperidinol-containing molecule is active against *Mycobacterium tuberculosis* by inhibiting the mycolic acid flippase activity of MmpL3, J. Biol. Chem. 294 (2019) 17512–17523. https://doi.org/10.1074/jbc.RA119.010135.
[58] S. Chen, Y. Zhou, Y. Chen, J. Gu, fastp: an ultra-fast all-in-one FASTQ preprocessor, Bioinformatics. 34 (2018) i884–i890. https://doi.org/10.1093/bioinformatics/bty560.
[59] D.E. Wood, J. Lu, B. Langmead, Improved metagenomic analysis with Kraken 2, Genome Biol. 20 (2019) 257. https://doi.org/10.1186/s13059-019-1891-0.

[60] A. Bankevich, S. Nurk, D. Antipov, A.A. Gurevich, M. Dvorkin, A.S. Kulikov, V.M. Lesin, S.I. Nikolenko, S. Pham, A.D. Prjibelski, A.V. Pyshkin, A.V. Sirotkin, N. Vyahhi, G. Tesler, M.A. Alekseyev, P.A. Pevzner, SPAdes: a new genome assembly algorithm and its applications to single-cell sequencing, J. Comput. Biol. 19 (2012) 455–477. https://doi.org/10.1089/cmb.2012.0021.

[61] L.G. Dover, A. Alahari, P. Gratraud, J.M. Gomes, V. Bhowruth, R.C. Reynolds, G.S. Besra, L. Kremer, EthA, a common activator of thiocarbamide-containing drugs acting on different mycobacterial targets, Antimicrob. Agents Chemother. 51 (2007) 1055–1063. https://doi.org/10.1128/AAC.01063-06.

Captions:

Table 1. MIC (µg/mL) values determined in either 7H9 broth supplemented with 10% OADC, 0.025% tyloxapol and 109 µM pantothenic acid against *M. tuberculosis* (*Mtb*) mc^26230 carrying the empty pMV261, *M. marinum* (*Mma*) M strain, and *M. abscessus* (*Mab*) $CIP104536^T$ (S and R variants). ND, non-determined.

Table 2. MIC (µg/mL) values were determined in 7H9 broth or 7H10 agar supplemented with 10% OADC and 109 µM pantothenic acid of the most potent analogs against *M. tuberculosis* mc^26230 overexpressing InhA.

Table 3. Spontaneous mutation frequency conferring resistance to **16g**, **16f** and **16d** in *M. tuberculosis* following exposure to 5x, 10x or 20x MIC. One resistant colony from each plate was subjected to PCR/sequencing of *katG*.

Figure 1: Design of synthesized hybrids based on anti-mycobacterial drugs/active molecules carrying a quinoline core and isoniazid.

Figure 2: Graphical representation of anti-mycobacterial SAR.

Figure 3. Growth of *M. tuberculosis* mc^26230 treated with the 16a-16g hybrids. Bacteria grown in 7H9 broth supplemented with 10% OADC, 0.025% tyloxapol and 109 µM pantothenic acid were incubated at 37 °C for 6 days with increasing drug concentrations corresponding to 1x MIC **(A)**, 5x MIC **(B),** and 20x MIC **(C)** of each compound. At different time points, CFU was determined by plating 10-fold dilutions of each culture onto Middlebrook 7H10 agar plates supplemented with 10%

OADC and pantothenic acid. The average of four independent experiments completed in technical triplicates is shown, with error bars representing standard deviations.

Figure 4. Cytotoxicity assay of INH, rifabutin, and 16a-16g in THP-1 cells. Cells were differentiated with PMA for 48 hrs and exposed to increasing concentration of each compound (starting at 100 µg/mL) for an additional 24 hrs (left panel) or 72 hrs (right panel) at 37°C with 5% CO_2. INH and RFB were included as reference drugs. Results are the mean of three independent experiments done in triplicates.

Figure 5. Inhibition of mycolic acid biosynthesis by 16g. *M. tuberculosis* $mc^2$6230 carrying either the empty pMV261 or the pMV261-*inhA* were treated with increasing concentrations of INH or **16g** in 7H9 broth supplemented with 10% OADC, 0.025% tyloxapol and 109 µM pantothenic acid at 37°C for 15 hrs with agitation. With agitation, the cultures were labeled with 1µCi/ml [^{14}C]acetate at 37°C for 7 hours. Following extraction, total mycolic acids and fatty acids were derivatized, and equal counts (50, 000 cpm) of the corresponding methyl esters were loaded onto a TLC plate. [^{14}C]-labeled lipids were separated after 2 runs in hexane/ethyl acetate (19/1, v/v) and exposed overnight.

Scheme 1: Synthesis of quinoline-based precursors **2-7.**

Scheme 2: Synthesis of Cu catalyzed 1*H*-1,2,3 triazolylquinoline derivatives **12-15** possessing free aldehyde group.

Scheme 3: Synthesis of 1*H*-1,2,3triazole-tethered quinoline-isoniazid hybrids **16a-g.**

Scheme 4: Synthesis of 1*H*-1,2,3triazole-tethered quinoline-nicotinoyl **17a-g** and quinoline-pyrazine-2-carbohydrazone **18a-g.**

Table 1. MIC[a] (µg/mL) values determined in either 7H9 broth against *M. tuberculosis* (*Mtb*) $mc^2$6230 carrying the empty pMV261, *M. marinum* (*Mma*) M strain, and *M. abscessus* (*Mab*) CIP104536^T (S and R variants). ND, non-determined.

Entry	clogP[b]	*Mtb*	*Mma*	*Mab*(S)	*Mab*(R)	Entry	clogP[b]	*Mtb*	*Mma*	*Mab*(S)	*Mab*(R)
12a	4.12	>200	ND	ND	ND	**17a**	4.26	>200	ND	ND	ND
12b	3.71	>200	ND	ND	ND	**17b**	3.85	>200	ND	ND	ND
13a	3.91	>200	ND	ND	ND	**17c**	4.04	>200	ND	ND	ND
13b	4.18	50	200	>200	>200	**17d**	4.31	>200	ND	ND	ND
13c	3.50	>200	ND	ND	ND	**17e**	3.63	>200	ND	ND	ND
13d	3.77	>200	ND	ND	ND	**17f**	3.90	>200	ND	ND	ND
14	3.60	100	>200	>200	>200	**17g**	3.74	>200	ND	ND	ND
16a	4.20	**0.25**	>200	>200	>200	**18a**	4.03	>200	ND	ND	ND
16b	3.79	**0.5**	>200	>200	>200	**18b**	3.62	>200	ND	ND	ND
16c	3.99	**0.5**	200	>200	>200	**18c**	3.81	ND	ND	ND	ND
16d	4.26	**0.5**	50	>200	>200	**18d**	4.08	>200	ND	ND	ND
16e	3.58	**0.5**	>200	>200	>200	**18e**	3.40	>200	ND	ND	ND
16f	3.85	**0.25**	100	>200	>200	**18f**	3.67	>200	ND	ND	ND
16g	3.68	**0.25**	50	>200	>200	**18g**	3.51	>200	ND	ND	ND
INH[c]		0.05	25	>200	>200	**6[d]**	2.23	92			

[a]MIC_{99}, Minimum inhibitory concentration that inhibits 99% of bacterial growth (µg/mL)
[b]clogP, lipophilicity parameter calculated from Molinspiration
[c]INH, isoniazid (reference drug)
[d]from reference [37]

Table 2. MIC (µg/mL) values were determined in 7H9 broth or 7H10 agar supplemented with 10% OADC and 109 µM pantothenic acidof the most potent analogs against *M. tuberculosis* $mc^2$6230 overexpressing InhA.

	MIC (µg/mL)			
	7H9 broth		7H10 agar	
Compound	**pMV261**	**pMV261-*inhA***	**pMV261**	**pMV261-*inhA***
16a	0.25	>200	0.25	6.25
16b	0.5	50	0.25	12.5
16c	0.5	12.5	0.25	6.25
16d	0.5	12.5	0.25	6.25
16e	0.5	25	0.5	12.5
16f	0.25	25	0.25	6.25
16g	0.25	6.25	0.25	6.25
INH	0.05	1	0.05	1

Table 3. Spontaneous mutation frequency conferring resistance to **16g**, **16f** and **16d** in *M. tuberculosis* following exposure to 5x or 20x MIC. One resistant colony from each plate was subjected to whole genome sequence or PCR/sequencing of *katG*.

Strain	Mutation frequency	Gene	SNP	AA change
Mtb-16g$^{R}_{5X}$	1.8 x 10^{-6}	*katG*	A1780C	F594C
Mtb-16g$^{R}_{20X}$	7.1 x 10^{-7}	*katG*	1_557del	186 del
Mtb-16f$^{R}_{5X}$	1.16 x 10^{-6}	*katG*	A480G	W161R
Mtb-16d$^{R}_{5X}$	1.52 x 10^{-6}	*katG*	665_666insC	Stop
Mtb-16d$^{R}_{20X}$	5 x 10^{-7}	*katG*	G1484A	G495D

Figure 1: Design of synthesized hybrids based on anti-mycobacterial drugs/active molecules carrying quinoline core and isoniazid.

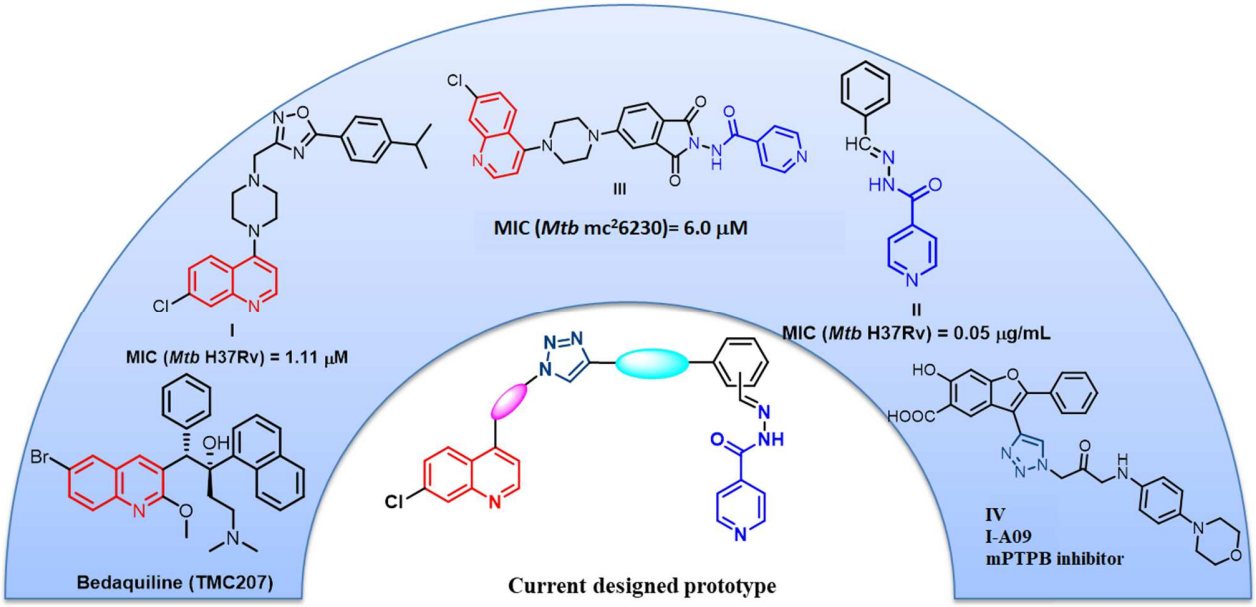

Figure 2: Graphical representation of anti-mycobacterial SAR.

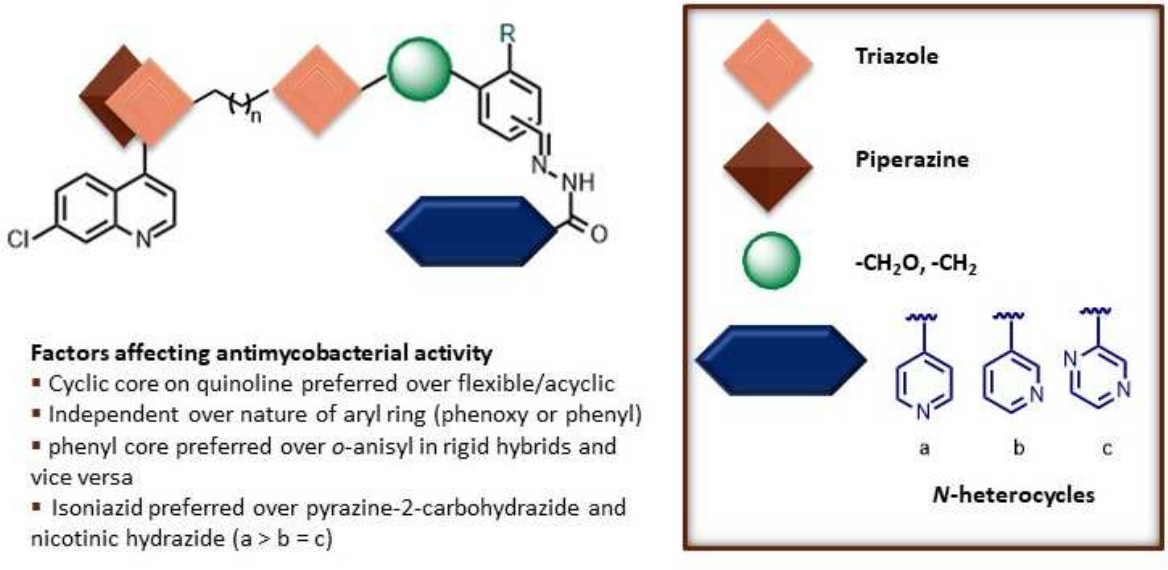

Figure 3. Growth of *M. tuberculosis* mc^{2}6230 treated with the 16a-16g hybrids. Bacteria grown in 7H9 broth supplemented with 10% OADC, 0.025% tyloxapol and 109 µM pantothenic acid were incubated at 37 °C for 6 days with increasing drug concentrations corresponding to 1x MIC **(A)**, 5x MIC **(B),** and 20x MIC **(C)** of each compound. At different time points, CFU was determined by plating 10-fold dilutions of each culture onto Middlebrook 7H10 agar plates supplemented with 10% OADC and pantothenic acid. The average of four independent experiments completed in technical triplicates is shown, with error bars representing standard deviations.

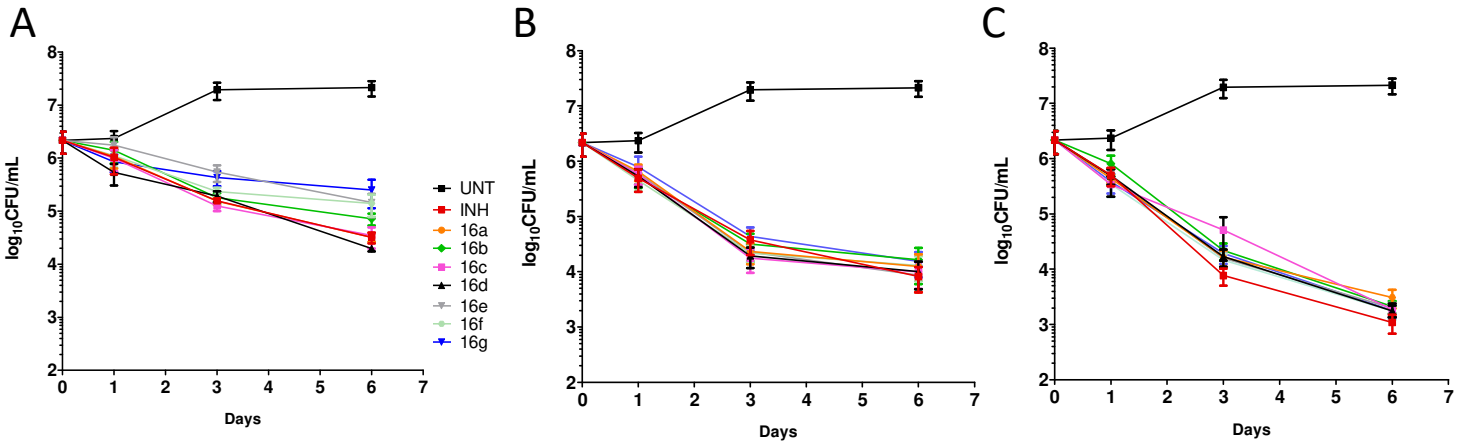

Figure 4. Cytotoxicity assay of INH, rifabutin, and 16a-16g in THP-1 cells. Cells were differentiated with PMA for 48 hrs and exposed to increasing concentration of each compound (starting at 100 µg/mL) for an additional 24 hrs (left panel) or 72 hrs (right panel) at 37°C with 5% CO_2. INH and RFB were included as reference drugs. Results are the mean of three independent experiments done in triplicates.

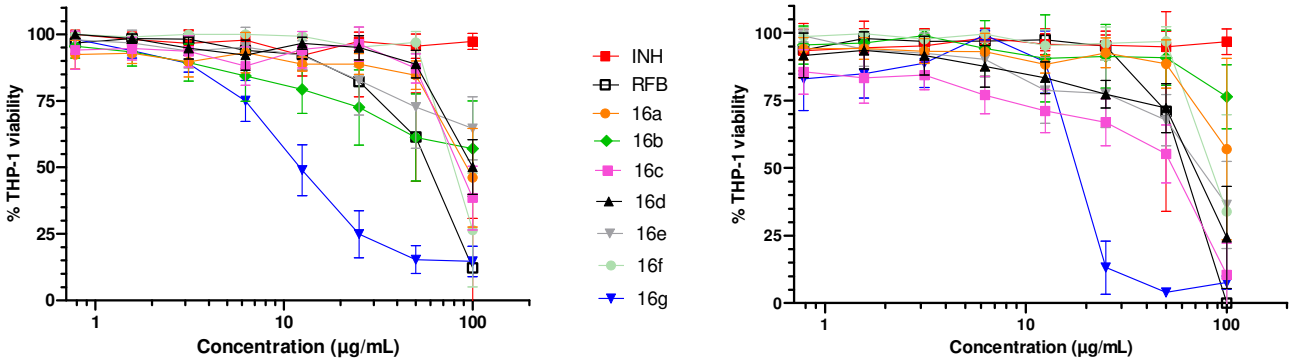

Figure 5. Inhibition of mycolic acid biosynthesis by 16g. *M. tuberculosis* mc^{2}6230 carrying either the empty pMV261 or the pMV261-*inhA* were treated with increasing concentrations of INH or **16g** in 7H9 broth supplemented with 10% OADC, 0.025% tyloxapol and 109 µM pantothenic acid at 37°C for 15 hrs with agitation. With agitation, the cultures were labeled with 1µCi/ml [^{14}C]acetate at 37°C for 7 hrs. Following extraction, total mycolic acids and fatty acids were derivatized and equal counts (50, 000 cpm) of the corresponding methyl esters were loaded onto a TLC plate. [^{14}C]-labeled lipids were separated after 2 runs in hexane/ethyl acetate (19/1, v/v) and exposed overnight.

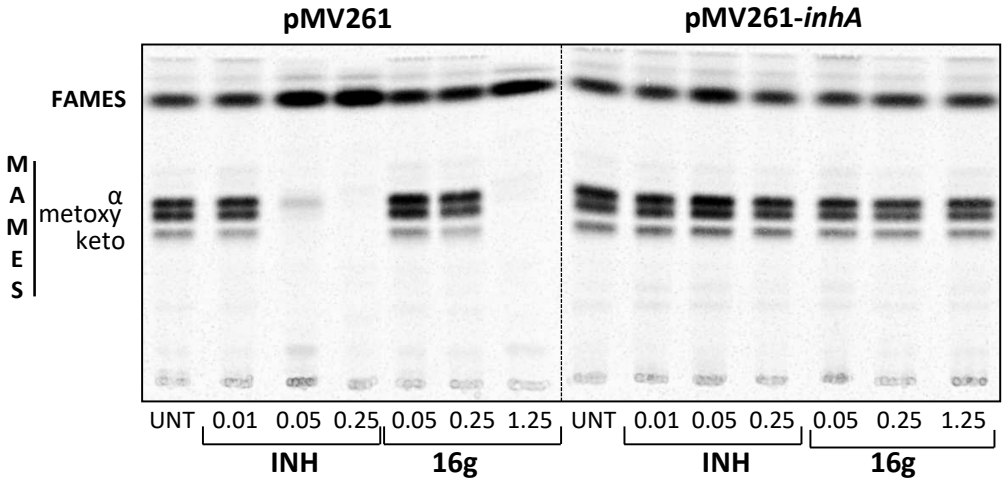

Scheme 1: Synthesis of quinoline-based precursors **2-7.**

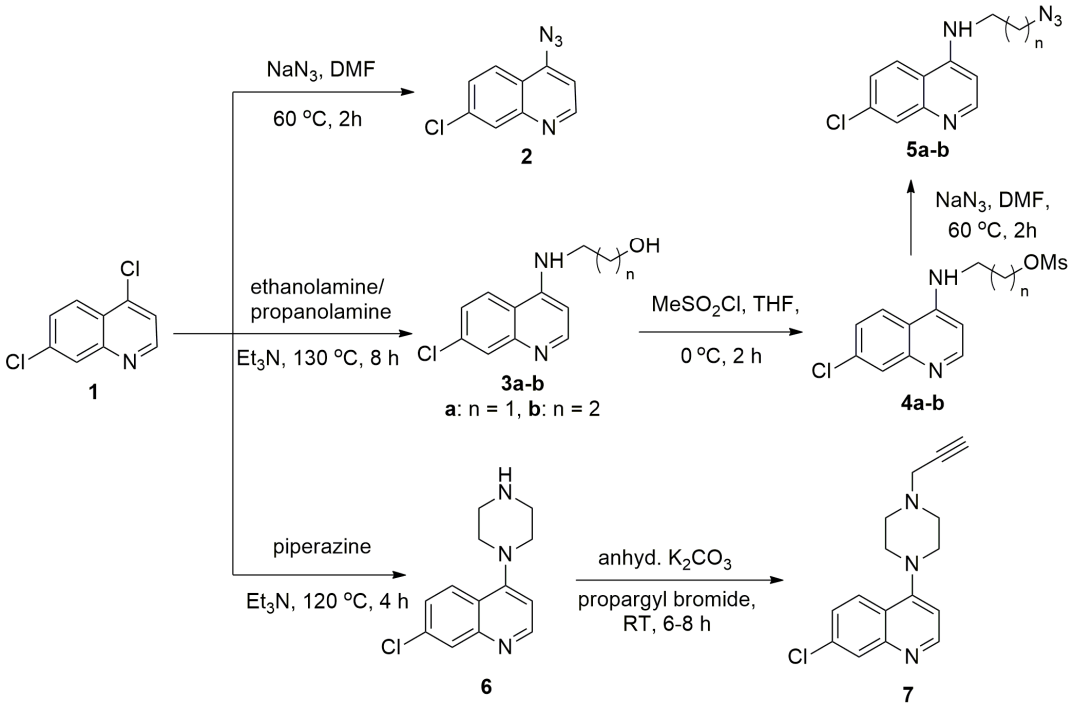

Scheme 2: Synthesis of Cu catalyzed 1*H*-1,2,3triazolylquinoline derivatives **12-15** possessing free aldehyde group.

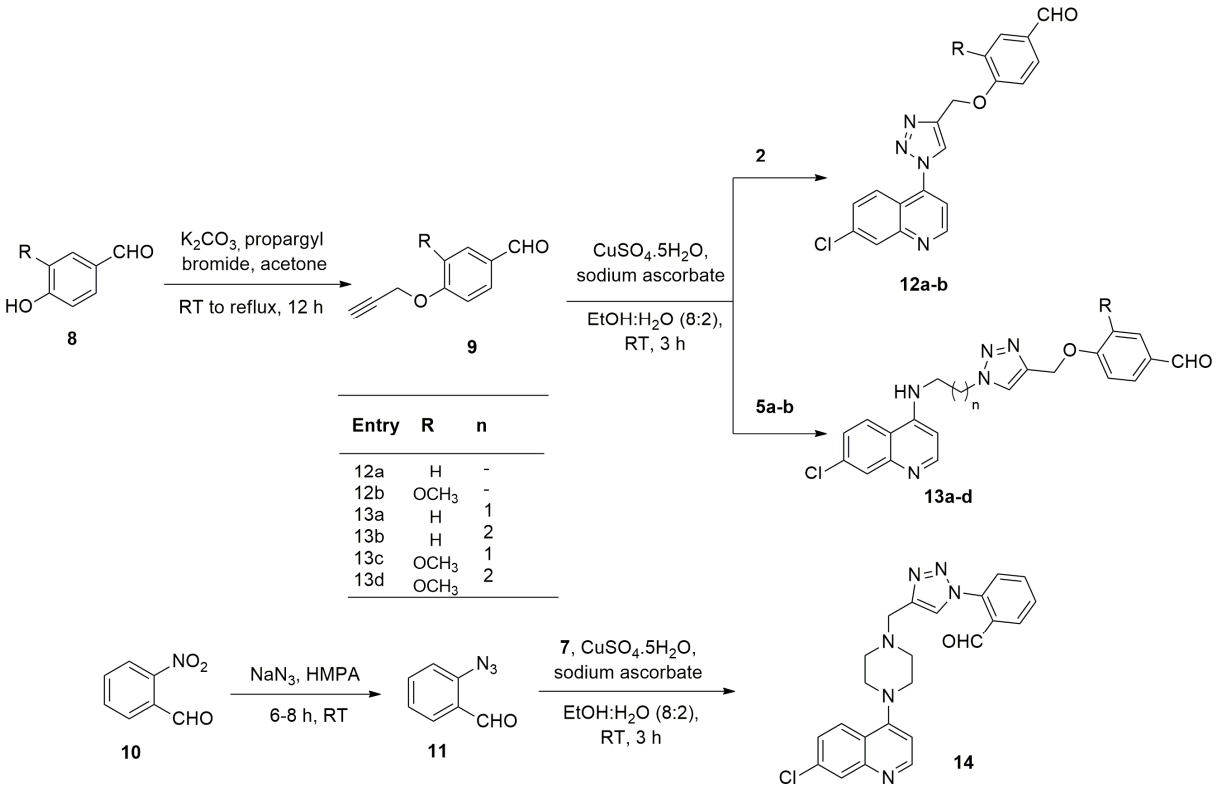

Scheme 3: Synthesis of 1*H*-1,2,3triazole-tethered quinoline-isoniazid hybrids **16a-g.**

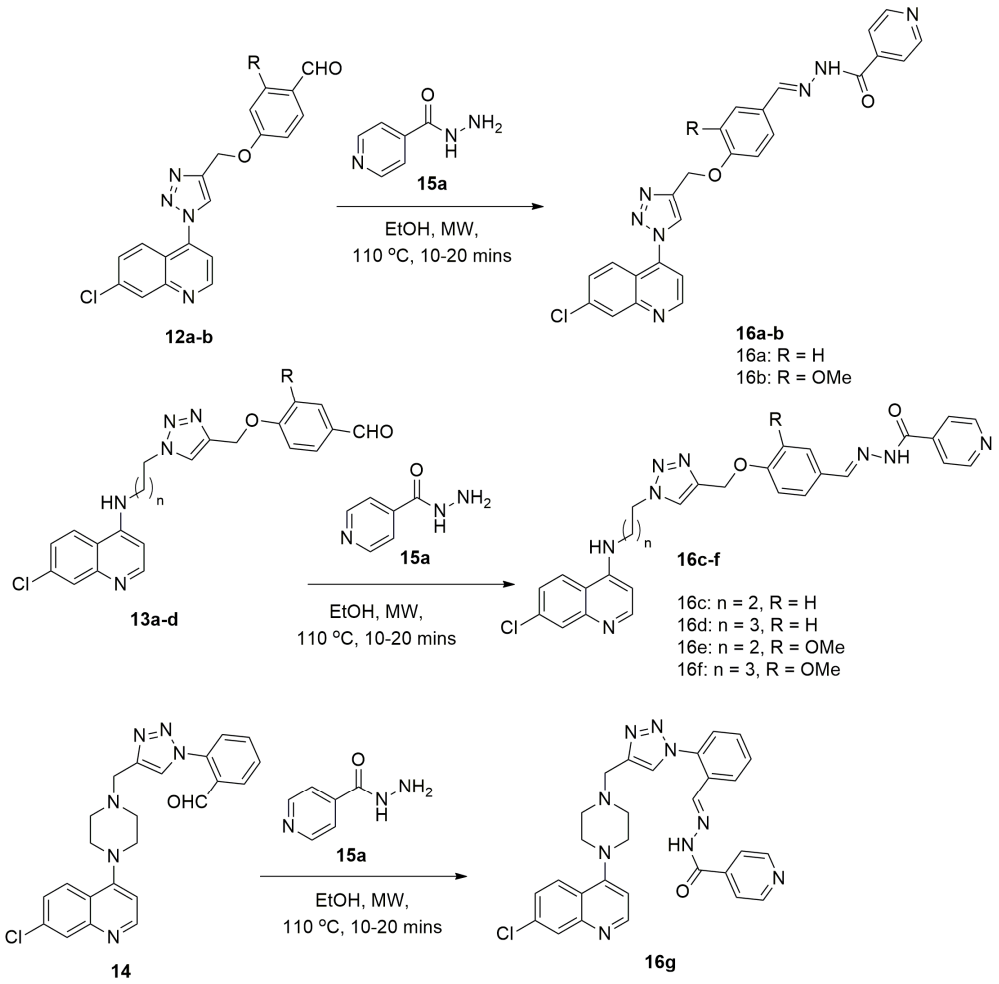

Scheme 4: Synthesis of 1*H*-1,2,3triazole-tethered quinoline-nicotinoyl**17a-g** and quinoline-pyrazine-2-carbohydrazone **18a-g.**

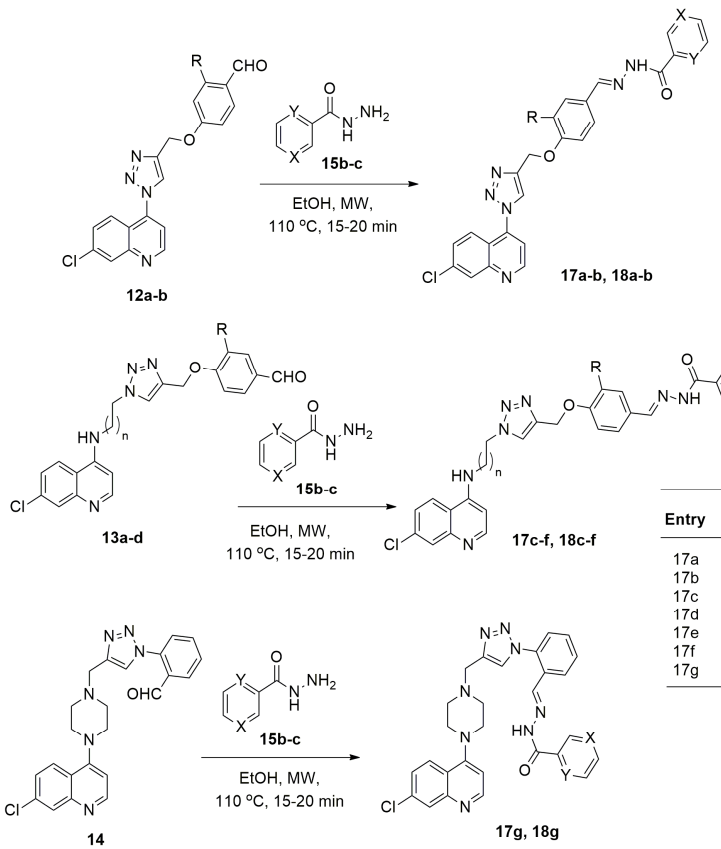

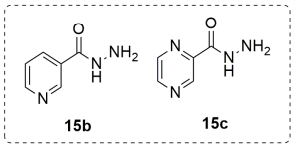

Entry	R	X	Y	n	Entry	R	X	Y	n
17a	H	N	H	-	18a	H	N	H	-
17b	OMe	N	H	-	18b	OMe	N	H	-
17c	H	N	H	2	18c	H	N	H	2
17d	H	N	H	3	18d	H	N	H	3
17e	OMe	N	H	2	18e	OMe	N	H	2
17f	OMe	N	H	3	18f	OMe-	N	H	3
17g	-	N	H	-	18g		N	H	-

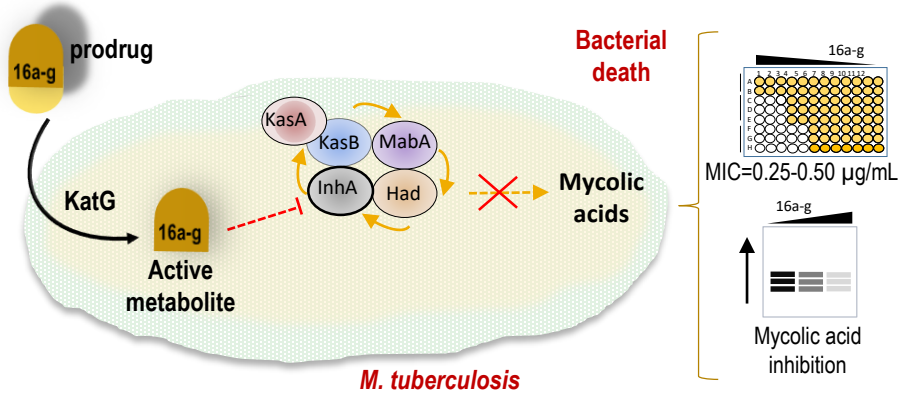
16a-g
prodrug
KatG
16a-g
Active metabolite
KasA
KasB
MabA
InhA
Had
Mycolic acids
Bacterial death
M. tuberculosis
16a-g
MIC=0.25-0.50 µg/mL
16a-g
Mycolic acid inhibition